Research

Induced ligno-suberin vascular coating and tyramine-derived hydroxycinnamic acid amides restrict *Ralstonia solanacearum* colonization in resistant tomato

Anurag Kashyap[1], Álvaro Luis Jiménez-Jiménez[1]*, Weiqi Zhang[1]*, Montserrat Capellades[1,2], Sumithra Srinivasan[3], Anna Laromaine[3], Olga Serra[4], Mercè Figueras[4], Jorge Rencoret[5], Ana Gutiérrez[5], Marc Valls[1,6] and Nuria S. Coll[1,2]

[1]Centre for Research in Agricultural Genomics (CRAG), CSIC-IRTA-UAB-UB, Campus UAB, 08193 Bellaterra, Spain; [2]Consejo Superior de Investigaciones Científicas (CSIC), 08001 Barcelona, Spain; [3]Institute of Material Science of Barcelona (ICMAB), CSIC, Campus UAB, 08193 Bellaterra, Spain; [4]Laboratori del Suro, Biology Department, University of Girona, Campus Montilivi, 17003 Girona, Spain; [5]Institute of Natural Resources and Agrobiology of Seville (IRNAS), CSIC, 41012 Seville, Spain; [6]Department of Genetics, University of Barcelona, 08028 Barcelona, Spain

Summary

• Tomato varieties resistant to the bacterial wilt pathogen *Ralstonia solanacearum* have the ability to restrict bacterial movement in the plant. Inducible vascular cell wall reinforcements seem to play a key role in confining *R. solanacearum* into the xylem vasculature of resistant tomato. However, the type of compounds involved in such vascular physico-chemical barriers remain understudied, while being a key component of resistance.

• Here we use a combination of histological and live-imaging techniques, together with spectroscopy and gene expression analysis to understand the nature of *R. solanacearum*-induced formation of vascular coatings in resistant tomato.

• We describe that resistant tomato specifically responds to infection by assembling a vascular structural barrier formed by a ligno-suberin coating and tyramine-derived hydroxycinnamic acid amides. Further, we show that overexpressing genes of the ligno-suberin pathway in a commercial susceptible variety of tomato restricts *R. solanacearum* movement inside the plant and slows disease progression, enhancing resistance to the pathogen.

• We propose that the induced barrier in resistant plants does not only restrict the movement of the pathogen, but may also prevent cell wall degradation by the pathogen and confer antimicrobial properties, effectively contributing to resistance.

Introduction

In natural environments plants are constantly exposed to diverse microbiota, including pathogenic organisms. In addition to pre-existing structural cell barriers that act as a first line of defense (Serrano *et al.*, 2014; Falter *et al.*, 2015), pathogen perception results in activation of a complex, multi-layered immune system in plants (Jones & Dangl, 2006). As part of the suite of inducible defenses, *de novo* formation of physico-chemical barriers prevents pathogen colonization and spread inside the plant. Despite their importance, the exact composition of these barriers, as well as the mechanisms that lead to their formation in the plant upon pathogen invasion remain largely unknown.

The interaction between the soil-borne bacterial wilt pathogen *Ralstonia solanacearum* and tomato offers a paradigmatic scenario to study inducible physico-chemical barriers, because of its agro-economic impact, and the well-developed genetic and molecular tools available in both organisms. *Ralstonia solanacearum* enters the root system through wounds or at the points of emergence of lateral roots, where the epidermal and endodermal barriers may be compromised (Vasse *et al.*, 1995; Álvarez *et al.*, 2010; Ursache *et al.*, 2021). After entering the root, the bacterium moves centripetally towards the vasculature and once it reaches the xylem, it multiplies and spreads vertically within the vessels and horizontally to other vessels and the surrounding tissues (Digonnet *et al.*, 2012).

The xylem tissue is a major battleground for the interaction between vascular wilt pathogens and their hosts, where the outcome of the infection is at stake (Yadeta & Thomma, 2013). To prevent the spread of pathogenic propagules, the xylem vasculature of resistant plants undergoes intense structural and metabolic modifications, such as reinforcing the walls of xylem vessels, pit membranes and surrounding xylem parenchyma cells in response to pathogens (Street *et al.*, 1986; Benhamou, 1995). This prevents pathogen colonization of the surrounding parenchyma

---

*These authors contributed equally to this work.

cells, nearby vessels and inter-cellular spaces through degeneration of the vessel pit membranes or cell walls by the pathogen (Nakaho *et al.*, 2000; Liu *et al.*, 2005; Pérez-Donoso *et al.*, 2010; Digonnet *et al.*, 2012; Lowe-Power *et al.*, 2018). This vascular confinement is an effective strategy commonly found among plants resistant to vascular wilt pathogens such as *R. solanacearum*, which otherwise spread systemically and eventually kill the plant (McGarvey *et al.*, 1999; Vasse *et al.*, 2000; Potter *et al.*, 2011; Caldwell *et al.*, 2017; Scortichini, 2020; Kashyap *et al.*, 2021).

Among the various tomato germplasms, the cultivar Hawaii 7996 (H7996) is the most effective natural source of resistance against *R. solanacearum* (Grimault *et al.*, 1994; Nakaho *et al.*, 2004). In this cultivar, resistance to *R. solanacearum* is a complex polygenic trait (2000; Thoquet *et al.*, 1996; Mangin *et al.*, 1999; Wang *et al.*, 2013). Our previous study identified the bottlenecks through which H7996 is able to limit *R. solanacearum* spread *in planta* (Planas-Marquès *et al.*, 2019), namely: (1) root colonization, (2) vertical movement from roots to shoots, (3) circular invasion of the vascular bundle and (4) radial apoplastic spread from the vessels into the cortex. Vascular cell wall reinforcements seem to play a key role in confining *R. solanacearum* into the xylem vascular bundles of resistant tomato H7996. Ultra-microscopic studies in resistant tomato showed that the pit membranes, as well as xylem vessel walls and parenchyma cells form a conspicuously thick coating in the form of an electron dense amorphous layer, as part of the defense response against *R. solanacearum* (Nakaho *et al.*, 2000; Kim *et al.*, 2016).

Among the polymers constituting vascular coating structures, lignin is the most typically found, constituting an integral part of the secondary cell wall of the xylem vasculature. Lignin is well documented as a common structural defense against vascular wilt pathogens (Novo *et al.*, 2017; Zeiss *et al.*, 2019; Kashyap *et al.*, 2021) and it is also emerging as an important inducible defense component in other diseases/pests affecting the vasculature (Jhu *et al.*, 2021; Joo *et al.*, 2021) Suberin has also been reported to be deposited in vascular coatings as a defense response (Kashyap *et al.*, 2021), although the mechanisms regulating its synthesis, spatio-temporal dynamics and inducibility remain elusive. Interestingly, root microbiota has been recently shown to shape suberin deposits in the plant, highlighting its central role in plant–microbe interactions (Salas-González *et al.*, 2021). Suberin is a polyester containing long and very long chain fatty acids and derivatives and also some aromatics, mainly ferulic acid. Cells that accumulate suberin also accumulate lignin, whose deposition has been described to precede that of suberin in phellem cells (Lulai & Corsini, 1998). This lignin is also known as a lignin-like polymer, which consists of hydroxycinnamates and mono-lignols (Graça, 2015). The ligno-suberin heteropolymer formed by the lignin-like polymer and suberin has been also referred to as the poly(aromatic) and poly(aliphatic) domains of suberin, respectively. Commonly, suberized cell walls also comprise soluble phenolic compounds, which share biosynthetic pathways with suberin and lignin (Bernards, 2002).

Ferulic acid present in the suberin and lignin-like fractions is proposed to link both polymers (Graça, 2010) and its continuous production has been demonstrated essential for suberin deposition (Andersen *et al.*, 2021). Ferulic acid amides, such as feruloyl-tyramine and feruloyloctopamine, have been described as structural components of the lignin-like polymer and in the phenolic soluble fraction of suberizing wound-healing potato tuber (Negrel *et al.*, 1996; Razem & Bernards, 2002). Ferulic acid amides belong to the hydroxycinnamic acid amide (HCAA) family, which present antimicrobial activity and are considered biomarkers during plant–pathogen interactions (Zeiss *et al.*, 2021). However, the precise role of HCAAs in plant defense remains to be elucidated (Macoy *et al.*, 2015a,b). Besides their direct antimicrobial activity as soluble phenols, HCAAs have also been proposed to crosslink to cell wall structural polymers during infection, potentially contributing towards the formation of a phenolic barrier that can make the cell wall resilient to pathogenic degradation (Zeiss *et al.*, 2021).

In the present study, we conducted a detailed investigation of the inducibility, structure and composition of the xylem vascular wall reinforcements that restrict *R. solanacerum* colonization in resistant tomato. Using a combination of histological and live-imaging techniques, together with spectroscopy and gene expression analysis we provide important new insights into the pathogen-induced formation of vascular coatings. In particular, we show that a ligno-suberin vascular coating and tyramine-derived HCAAs contribute to restriction of *R. solanacearum* in resistant tomato. In addition, we demonstrate that genes in the ligno-suberin-associated pathways can be explored to engineer resistance against *R. solanacearum* into commercial susceptible varieties of tomato.

Materials and Methods

Plant materials and growth conditions

Tomato (*Solanum lycopersicum*) varieties Marmande, Hawaii 7996 (H7996) and Moneymaker (wild-type and *35S::THT 1-3*, generated by Campos *et al.* (2014)), were used. Plants were grown in controlled growth chambers at 60% humidity, 12 h : 12 h, day : night and 27°C (light-emitting diode (LED) lighting) or 25°C (fluorescent lighting).

Ralstonia solanacearum strains and growth conditions

Ralstonia solanacearum GMI1000 strain (Phylotype I, race 1 biovar 3) was used, including luminescent and fluorescent reporter strains of *R. solanacearum* GMI1000 described in Cruz *et al.* (2014) and Planas-Marquès *et al.* (2019).

Cloning and stable transformation in tomato

For generation of the *35S::FHT-HA* construct the *FHT* (Soly-c03g097500) coding sequence was amplified from tomato H7996 complementary DNA (cDNA) using the forward and reverse primers part7FHTF1 and part7FHTHAR1, respectively (Supporting Information Table S1). The amplified product was cloned into the pJET1.2/blunt cloning vector using a CloneJet

PCR cloning kit (ThermoFisher, Waltham, MA, USA) and then digested by *Sma*I and *Bam*HI. The digested products were purified using NZYGelpure (Nzytech, Lisbon, Portugal) followed by ligation into the pART7 and later to pART27 vector (Gleave, 1992). pART27 containing *35S::FHT-HA* was transformed into Marmande. For this, the construct was transformed into *Agrobacterium tumefaciens* strain C58C1. Cotyledon explant preparation, selection, and regeneration followed the methods described by Mazier *et al.* (2011). Transformants were selected on kanamycin-containing medium. Accumulation of FHT-HA protein was assayed by immunoblot with a monoclonal HA antibody (GenScript, Piscataway, NJ, USA).

Bacterial inoculation in plants

Four- to five-week-old tomato plants were inoculated through roots with *R. solanacearum* using the soil drenching method with a 1×10^7 colony-forming unit (CFU) ml^{-1} suspension of bacteria as described in Planas-Marquès *et al.* (2018). Inoculated plants were kept in a growth chamber at 27°C. For tomato leaf infiltration, plants were vacuum-infiltrated by submerging the whole aerial part in a *c.* 10^5 CFU ml^{-1} bacterial suspension as described in Planas-Marquès *et al.* (2018). For inoculation directly onto the stem vasculature, 10 µl (5 µl at a time) of 10^5 CFU ml^{-1} bacterial suspension was placed at the node of the petiole and pin-inoculated using a sterile needle (30G × ½″, BD Microlance; Becton Dickinson, Franklin Lakes, NJ, USA).

Ralstonia solanacearum pathogenicity assays and quantification of bacterial growth *in planta*

Infected plants were scored for wilting symptoms using a scale from 0 to 4: 0 = healthy plant with no wilt, 1 = 25%, 2 = 50%, 3 = 75%, and 4 = 100% of the canopy wilted as described by Planas-Marquès *et al.* (2019). The relative light units per second (RLU s^{-1}) readings were converted to CFU g^{-1} tissue as described in Planas-Marquès *et al.* (2019). For bacterial colonization assays using green fluorescent protein (GFP) reporter strain, transverse stem cross-sections were made at the inoculation point and at a distance of 0.5, 1, 2 and 3 cm in both upward and downward direction, using a sterile razor blade. Quantification of mean green fluorescence was done using IMAGEJ software (Planas-Marquès *et al.*, 2019). For leaf *in planta* multiplication assays, three leaf discs of 0.8 cm^2 were homogenized in 200 µl of sterile distilled water. CFU cm^{-2} leaf tissue were calculated after dilution plating of samples with appropriate selection antibiotics and CFU counting 24 h later.

Histological methods

Thin (*c.* 150 µm) transverse cross-sections were obtained with a sterile razor blade from a 1.5 cm area of the taproot-to-hypocotyl transition zone located immediately below the soil line (Fig. S1a). Inoculated plants were sectioned when bacterial colonization level reached 10^5 CFU g^{-1} taproot-to-hypocotyl transition zone tissue. This corresponded to 4 d post-inoculation (dpi) in

Marmande and 9 dpi in H7996, at which stage only H7996 sections showed a localized browning at one xylem pole indicative of infection. Sections were kept in 70% ethanol at room temperature for 5 d and examined using fluorescence microscopy using a Leica DM6B-Z microscope under ultraviolet (UV) illumination (340–380 nm excitation and 410–450 nm barrier filters). Autofluorescence emitted from phenolic deposits was recorded using a Leica-DFC9000GT-VSC07341 camera and the signal was pseudo-colored green. Sections were also stained with phloroglucinol-HCl for the detection of lignin and observed under bright field (Pomar *et al.*, 2004). Photographs were taken with a DP71 Olympus digital camera. Cross-sections were also observed under UV with a Leica-DM6B-Z microscope (340–380 nm excitation and 410–450 nm barrier filters). To detect the autofluorescent blue-to-green pH-dependent color conversion of wall-bound ferulic acid cross-sections were initially mounted in 70% ethanol (neutral pH) and then in 1N potassium hydroxide (KOH) (pH above 10) adapting the protocol from Carnachan & Harris (2000), Harris & Trethewey (2010) and Donaldson & Williams (2018). A Leica DM6B-Z microscope was used to observe autofluorescence (340–380 nm excitation and 410–450 nm barrier filters). Images were recorded using a Leica MC190-HD-0518131623 digital camera. To visualize suberin aliphatics, sections were treated with 5% Sudan IV, dissolved in 70% ethanol and illuminated with UV light. These sections were subsequently treated with 1N KOH to detect ferulic acid as described earlier. For both ferulic acid and suberin, the HC PL APO or HC PL FLUOTAR objectives of the Leica DM6B-Z microscope were used and images were captured using a Leica MC190-HD-0518131623 color digital camera. The UV autofluorescence signal from xylem vessel walls and surrounding layers was measured using the LAS X Leica software and changes in ferulate accumulation were quantified using IMAGEJ software by selecting the area of xylem vessel walls showing autofluorescence. Quantifications of fluorescence intensity were normalized per micrometer of region of interest (ROI), which corresponded to a particular area of the vascular bundles, where main vessels concentrate (represented in Fig. 1b). Basically, the line is drawn at each of the four corners in the whole image and then the fluorescence is normalized by the length of the lines.

Two-dimensional nuclear magnetic resonance (2D-NMR)

The samples of a pool of 15 tomato plants (taproot-to-hypocotyl region), water treated or having a bacterial load of 10^5 CFU g^{-1} were milled and extracted sequentially with water, 80% ethanol, and with acetone, by sonicating in an ultrasonic bath during 30 min each time, centrifuging and eliminating the supernatant. Then, lignin/suberin fraction was enzymatically isolated by hydrolyzing the carbohydrates fraction with Cellulysin (Calbiochem, San Diego, CA, USA), as previously described (Rico *et al.*, 2014). Approximately 20 mg of enzymatic lignin/suberin preparation was dissolved in 0.6 ml of deuterated dimethyl sulfoxide (DMSO-d_6). Heteronuclear single quantum coherence (HSQC) spectra were acquired on a Bruker Advance III 500 MHz spectrometer (Bruker, Karlsruhe, Germany) equipped
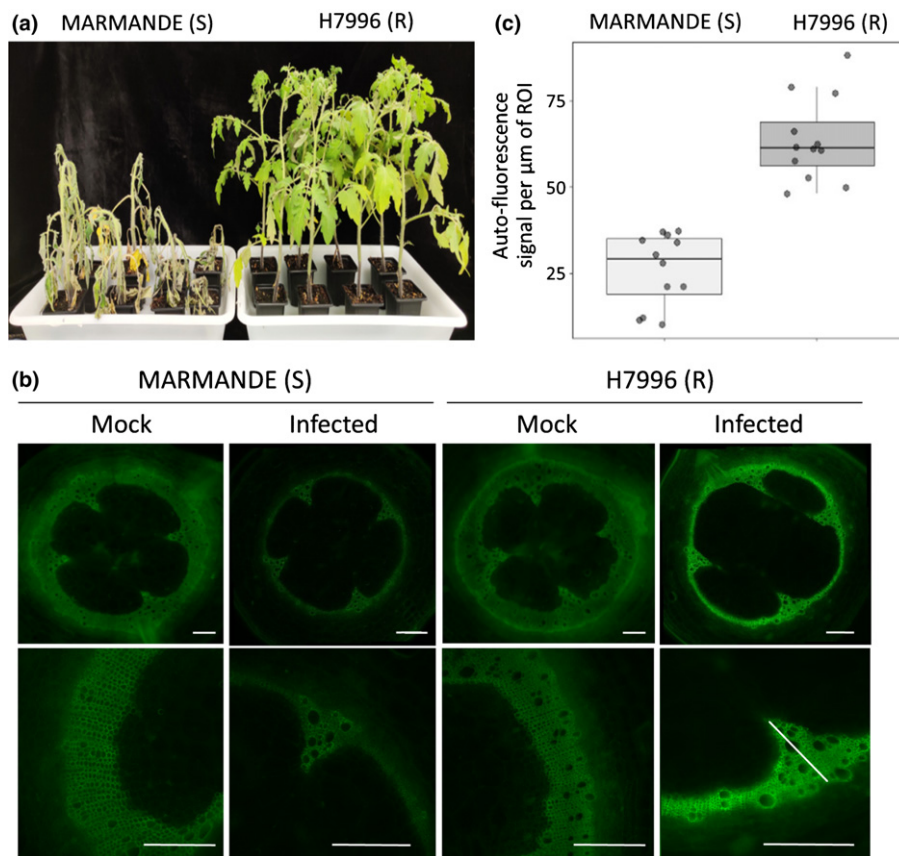
Fig. 1 Resistant H7996 tomato restricts *Ralstonia solanacearum* colonization and induces a vascular coating response with wall bound phenolics. Susceptible (Marmande) and resistant (H7996), 5-wk-old tomato plants were inoculated through roots by soil-soak with *c.* 1×10^7 colony-forming unit (CFU) ml^{-1} of *R. solanacearum* GMI1000 and incubated at 28°C. (a) At 12 d post-inoculation (dpi) most Marmande plants showed severe wilting symptoms, whereas H7996 remained mostly symptomless. (b) Cross-sections of the taproot-to-hypocotyl area containing 10^5 CFU g^{-1} of *R. solanacearum* were analyzed by ultraviolet (UV) microscopy. To focus on cell wall-deposited phenolic compounds, soluble phenolic compounds were removed with ethanol prior to observation. A strong autoflorescence signal emitted from the walls of vessels and surrounding parenchyma cells in infected H7996 plants compared to Marmande or the mock controls can be observed. Fluorescence signal in white was green colored. Images from a representative experiment out of three with *n* = 5 plants per cultivar. Bar, 500 µm. (c) The UV autofluorescence signal in (b) was measured using the Leica APPLICATION SUITE X (LAS X) software. A representative region of interest (ROI) is highlighted in (b) and corresponded to a line traversing the selected vascular bundles. Data are represented with box and whiskers plots: whiskers indicate variability outside the upper and lower quartiles and boxes indicate second quartile, median and third quartile. Different letters indicate statistically significant differences (α = 0.05, Fisher's least significant difference test).

with a 5 mm TCI cryoprobe, using the experimental conditions previously described (Rico *et al.*, 2014). HSQC cross-signals were assigned and quantified as described (del Río *et al.*, 2018; Rencoret *et al.*, 2018; Mahmoud *et al.*, 2020). In the aromatic region, the correlation signals of G_2 and $S_{2,6}$ were used to estimate the content of the respective G- and S-lignin units. The C_α/H_α signals of the β–*O*–4′ ethers (A_α), phenylcoumarans (B_α), and resinols (C_α) in the linkages region were used to estimate their relative abundances, whereas the C_γ/H_γ signal was used in the case of cinnamyl alcohol end-units (I_γ).

RNA extraction, cDNA synthesis and quantitative RT-PCR analysis

Taproot-to-hypocotyl transition zone sections of *c.* 0.5 mm thickness were obtained and the xylem vascular tissues (vascular bundles and surrounding parenchyma cells) were collected and kept in liquid nitrogen. Each sample comprised taproot-to-hypocotyl transition

zone xylem tissues of six plants. RNA was extracted using the Maxwell RSC Plant RNA Kit (Promega, Madison, WI, USA). Complementary DNA was synthesized from 2 µg RNA using High Capacity cDNA Reverse Transcription Kit (Applied Biosystems, Foster City, CA, USA). Complementary DNA amplification and analysis was performed using the LightCycler 480 System (Roche, Basel, Switzerland). The Elongation Factor 1 alpha housekeeping gene (*eEF1 α, Solyc06g005060*) was used as a reference. All reactions were run in triplicate for each biological replicates. Melting curves and relative quantification of target genes were determined using the software LIGHTCYCLER v.1.5 (Roche). The level of expression relative to the reference gene was calculated using the formula $2^{-\Delta CT}$, where ΔCT = (CT RNA target − CT reference RNA).

Statistical analysis

Statistical analyses were performed using STATGRAPHICS software. All statistical tests are indicated in the respective figure legends.

Results

Resistant H7996 tomato restricts *R. solanacearum* colonization and induces a vascular coating response involving wall-bound phenolics

In order to understand the mechanisms underscoring restriction of *R. solanacearum* spread in resistant tomato varieties we used the resistant variety H7996 and compared it to the susceptible cultivar Marmande. In our assay conditions, most Marmande plants were wilted 10 d after inoculation with *R. solanacearum* GMI1000, while H7996 plants remained largely asymptomatic (Figs 1a, S2a; Planas-Marquès *et al.*, 2019). Accordingly, bacterial loads in the taproot-to-hypocotyl region were drastically reduced in H7996 compared to Marmande, confirming the remarkable bacterial restriction ability of this cultivar (Fig. S1b; Planas-Marquès *et al.*, 2019).

To identify defense-associated anatomical and physico-chemical modifications in H7996 after infection with *R. solanacearum* compared to Marmande we performed histo-chemical, spectroscopic and gene expression analysis. For this, plants were infected with a 10^7 *R. solanacearum* solution or mock through their roots using the soil-drench method and then we collected tissue containing 10^5 CFU g^{-1} tissue of bacteria at the taproot-to-hypocotyl transition area, located *c.* 1 cm below-ground (Fig. S1a). Marmande reached 10^5 CFU g^{-1} tissue at around 4 dpi, while the resistant H7996 took approximately 9 d to do so (Fig. S2). We have previously observed that the root-to-hypocotyl area constitutes a key bottleneck for bacterial progression inside the plant (Zuluaga *et al.*, 2015; Puigvert *et al.*, 2017; Planas-Marquès *et al.*, 2019), being thus an ideal target zone for analysis of structural defense responses.

We initially analyzed UV autofluorescence of transverse cross-sections of the taproot-to-hypocotyl region, indicative of phenolic compounds (Donaldson, 2020). To focus on cell wall-deposited phenolic compounds, soluble phenolic compounds were removed with ethanol prior to observation as reported (Pouzoulet *et al.*, 2013; Araujo *et al.*, 2014). Infection with *R. solanacearum* induced a strong UV signal emitted from the walls of the vessels, and also from surrounding xylem parenchyma cells and tracheids in resistant H7996 (Fig. 1b,c). This enhanced autofluorescence was not observed in the susceptible variety Marmande nor in mock-treated samples (Fig. 1b, c). In tissues outside the vascular area, inoculation resulted in a decrease of autofluorescence in both susceptible and resistant tomato lines.

Spectroscopic analysis reveals *R. solanacearum*-induced deposition of suberin and accumulation of tyramine-derived amides in resistant H7996 tomato and lignin structural modifications in susceptible Marmande tomato

In order to decipher the composition of the cell wall-deposited compounds we used two-dimensional (2D) HSQC nuclear magnetic resonance (NMR), one of the most powerful tools for plant cell wall structural analysis providing information on the composition and linkages in lignin/suberin polymers (Ralph & Landucci, 2010; Correia *et al.*, 2020). The 2D-HSQC spectra of infected or mock-treated taproot-to-hypocotyl transition zones of H7996 and Marmande tomato plants were obtained and the main lignin and suberin substructures identified are shown in Fig. 2, while the chemical shifts of the assigned cross-signals are detailed in Table S2. Importantly, the aliphatic region of the 2D-HSQC spectra revealed that H7996 infected plants were more enriched in poly-aliphatic structures characteristic of suberin (magenta-colored signals), compared to its mock control (Fig. 2a). Related to this, an olefinic cross-signal of unsaturated fatty acid structures (UF, δ_C/δ_H 129.4/5.31), typical of suberin, was also found to be increased in the HSQC spectrum of the infected H7996 tomato. A rough estimate based on the integration of lignin and suberin HSQC signals, revealed that the suberin/lignin ratio in *R. solanacearum-infected* H7996 plants was doubled compared to mock-treated plants, evidencing an increase in suberin deposition as a consequence of the bacterial infection. Interestingly, signals compatible with feruloylamides (FAm$_7$; δ_C/δ_H 138.6/7.31) and with tyramine-derived amides (Ty in orange; δ_C/δ_H 129.3/6.92, 114.8/6.64, 40.5/3.29 and 34.2/2.62) were exclusively found in the spectrum of infected H7996 plants, suggesting the presence of feruloyltyramine exclusively in these samples (Fig. 2a). Since tyramines have been found as structural components co-occurring with suberin (Bernards *et al.*, 1995; Bernards & Lewis, 1998), which generates physically and chemically resistant barriers (He & Ding, 2020), our results substantiate the hypothesis of suberin as an important defense element against *R. solanacearum* infection in resistant tomato plants. On the contrary, the 2D-HSQC spectra from the Marmande variety did not display notable variations between mock and infected plants in the signals corresponding to suberin, tyramine-related structures nor feruloylamides (Fig. 2a).

Interestingly, 2D-HSQC-NMR spectra also revealed significant structural modifications in the composition of lignin and the distribution of linkages in tomato plants after infection. Lignins with lower S : G ratios are more branched (condensed) and recalcitrant towards pathogen attack (Iiyama *et al.*, 2020). Therefore, lignin in inoculated H7996, with an S : G ratio of 1.0 should be, a priori, more resistant than the lignin in inoculated Marmande plants (S : G ratio of 1.5). The 2D-HSQC analysis revealed that the infection of susceptible Marmande plants resulted in an increase of the S : G ratio and a clear reduction of all major lignin linkages (β–O–4′, β–5′ and β–β′; reduction in roughly 9%, 43% and 46%, respectively), evidencing that a lignin depolymerization process took place (Fig. 2a). In contrast, infected H7996 tomato displayed a slight decrease of the S : G ratio, and only β-O-4′ linkages (the easiest to degrade in the lignin polymer) were significantly reduced, while the β–5′ and β–β′ were not so affected as in the case of Marmande plants. In this context, the major reduction in lignin linkages observed in Marmande after infection could explain, at least in part, its higher susceptibility to the pathogen.
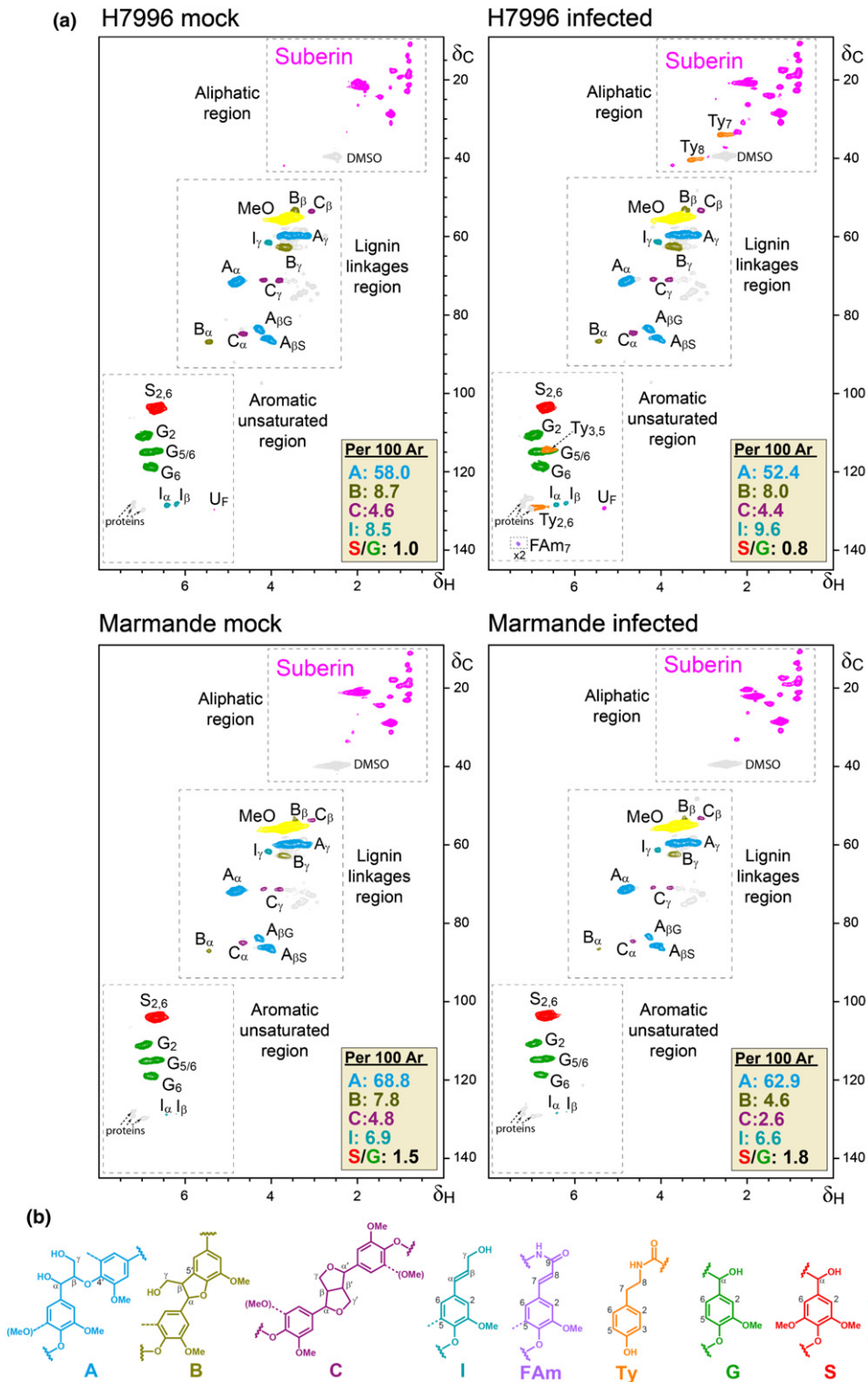
Fig. 2 Feruloylamides, tyramine-derived amides and suberin-compatible compounds are specifically enriched in resistant H7996 tomato after infection with *Ralstonia solanacearum*. (a) Two-dimensional heteronuclear single quantum correlation-nuclear magnetic resonance (2D-HSQC-NMR) spectra of enzymatically isolated lignin/suberin fractions from mock-treated and *R. solanacearum-infected* taproots (containing 10^5 colony-forming unit (CFU) g^{-1} taproot-to-hypocotyl transition tissue) of H7996 and Marmande tomato plants. The experiment was performed twice with similar results. (b) Main lignin/suberin structures identified: β–O–4′ alkyl aryl ethers (A), β–5′ fenylcoumarans (B), β–β′ resinols (C), cinnamyl alcohols end-groups (I), feruloylamides (FAm), tyramine-derived amides (Ty), guaiacyl lignin units (G), syringyl lignin units (S), as well as unassigned aliphatic signals from suberin. The structures and contours of the HSQC signals are color coded to aid interpretation. Proton (^{1}H) and carbon-13 (^{13}C) NMR chemical shifts of the assigned signals are detailed in Supporting Information Table S2. To detect FAm$_7$ signal, the spectrum scaled-up to 2-fold (×2) intensity. The abundances of the main lignin linkages (A, B and C) and cinnamyl alcohol end-groups (I) are referred to as a percentage of the total lignin units (S + G = 100%).

Histochemical analysis reveals the formation of structural vascular coatings containing suberin and ferulate/feruloylamide in resistant H7996 tomato in response to *R. solanacearum* infection

To confirm our spectroscopic data, we histochemically analyzed taproot-to-hypocotyl transition zone samples of mock and infected H7996 and Marmande tomato plants. Observation of Phloroglucinol-HCl stained sections under brightfield microscopy (Wiesner staining) (Pomar *et al.*, 2002; Pradhan Mitra & Loqué, 2014), showed that mock and infected H9776 (resistant) as well as mock Marmande (susceptible) samples showed a red-purple color characteristic of the reaction of phloroglucinol-HCl in vessels and fibers, indicative of lignin (Fig. 3a). In contrast, infected Marmande sections exhibited reduced phloroglucinol-HCl staining, suggesting a change in composition of xylem lignin upon infection (Fig. 3a). This observation is in agreement with the structural changes specifically detected in the lignin structure of infected Marmande plants by 2D-HSQC-NMR (Fig. 2a), which suggest lignin depolymerization and may partly underscore the high susceptibility of this tomato variety.

UV illumination of phloroglucinol-HCl-stained samples allows quenching the autofluorescence from lignin and hence detect residual cell wall autofluorescence, which has been associated with suberin deposits (Baayen & Elgersma, 1985; Rioux *et al.*, 1998; Pouzoulet *et al.*, 2013). Under these conditions, the increased autofluorescence observed in the vascular coating regions of infected H7996 tomato plants was not quenched in phloroglucinol-HCl stained samples (Fig. 3a,b). A more detailed observation revealed that this nonquenched autofluorescence was localized in specific regions compatible with (1) intervessel and vessel-parenchyma pit membranes or pit chamber walls and (2) parenchyma coatings with fluorescent signals enriched in intracellular spaces (Fig. 3c).

Next, we analyzed whether the pathogen-induced coating of vessels observed in H7996 correlated also with an increase in ferulates, a major suberin component. We performed KOH treatment of plant tissues, which specifically shifts the UV fluorescence of ferulate/feruloylamide to green, allowing its detection (Carnachan & Harris, 2000; Harris & Trethewey, 2010; Donaldson & Williams, 2018). UV autofluorescence of vascular coatings in response to *R. solanacearum* infection in resistant H7996 shifted from blue to a strong green color upon treatment with alkali (1N KOH) (Fig. S3a). This indicated that the *R. solanacearum*-induced xylem vasculature feruloylation was specific to resistant H7996, as the fainter blue autofluorescence observed in mock-treated resistant H7996 or susceptible Marmande tissues did not change to green at high pH in either early (Fig. S3a,b) or late (Fig. S3c) stages of infection.

To corroborate that the ferulate/feruloylamide accumulation in infected H7996 tomato was related with vascular suberization, we combined the ferulate-specific UV-alkali treatment described earlier with Sudan IV staining, which binds aliphatic components of suberin to produce a reddish-brown coloration. This revealed suberization in the taproot-to-hypocotyl area of *R. solanacearum*-infected H7996 plants, xylem vessel walls as well as the layers of

vessels, parenchyma cells and tracheids in the immediate vicinity (Fig. 4). In the periphery of suberized cells, a green signal from UV-alkali was observed (Fig. 4), which may indicate ferulate/feruloylamide deposition indicative of a preceding stage towards suberization in this cell layer. In comparison, no positive Sudan IV or UV-alkali staining was detected in infected Marmande or mock-treated tomato plants. Together, suberized and feruloylated layers of parenchyma cells, vessels and tracheids might form a 'suberization zone' creating a strong physico-chemical barrier to limit *R. solanacearum* spread from the colonized xylem vessel lumen.

Ralstonia solanacearum infection activates the biosynthesis of aliphatic suberin precursors and feruloylamide, and aliphatic esterification of ferulic acid in the vasculature of resistant H7996

Since a differential accumulation of suberin-compatible compounds was specifically observed in infected H7996, we surmised that genes related to suberin and feruloylamide synthesis, as well as ferulic acid esterification to aliphatics may be upregulated in resistant tomato in response to *R. solanacearum* invasion. To test this hypothesis, we analyzed: (1) expression of genes in the phenylpropanoid and suberin biosynthesis pathways, which provide the necessary precursors for the ligno-suberin heteropolymer; (2) the feruloyl transferase FHT (ASFT/HHT in Arabidopsis), which is involved in the formation of ferulate esters of fatty acyl compounds necessary to form suberin and soluble waxes (Gou *et al.*, 2009; Molina *et al.*, 2009; Serra *et al.*, 2010); and (3) N-hydroxycinnamoyl transferases (*THT*), which are involved in the synthesis of HCAAs such as feruloyltyramine, which is found on the lignin-like polymer and in the soluble phenolic fraction of some suberized tissues (Negrel *et al.*, 1993; Schmidt *et al.*, 1999).

Quantitative reverse transcription polymerase chain reaction (RT-PCR) from xylem vascular tissue obtained from the taproot-to-hypocotyl zone in *R. solanacearum*- or mock-treated H7996 and Marmande plants showed specific upregulation of all genes analyzed from the suberin biosynthetic pathway in H7996 infected plants compared to the mock controls (Figs 5, S4). These included essential suberin biosynthesis genes such as *CYP86A1* and *CYP86B1* (fatty acid oxidation), *FAR* (primary alcohol generation), *KCSs* (fatty acid elongases) and *GPAT5* (acylglycerol formation). In addition, feruloyl transferase *FHT* (*ASFT/HHT* in Arabidopsis), was also strongly upregulated in infected H7996 plants (Figs 5, S5b). Regarding *THT*, in tomato we identified five putative homologs (Fig. S6a), all induced by infection in the vascular tissue of H7996 (Figs 5, S6b). Among them, *SlTHT1-3* showed the strongest upregulation in H7996 after infection (Figs 5, S6b). In comparison, *R. solanacearum* infection had only a modest effect on genes related to phenylpropanoid pathway as only upregulation was detected in the first enzyme of the pathway (PAL) (Figs 5, S7).

Together, these data indicate that upregulation of genes involved in the formation of aliphatic suberin precursors, ferulic acid esterification to aliphatics (FHT) and production of HCAAs, such as feruloyltyramine (THT), constitute a very specific response of H7996 plants that takes place in the vasculature
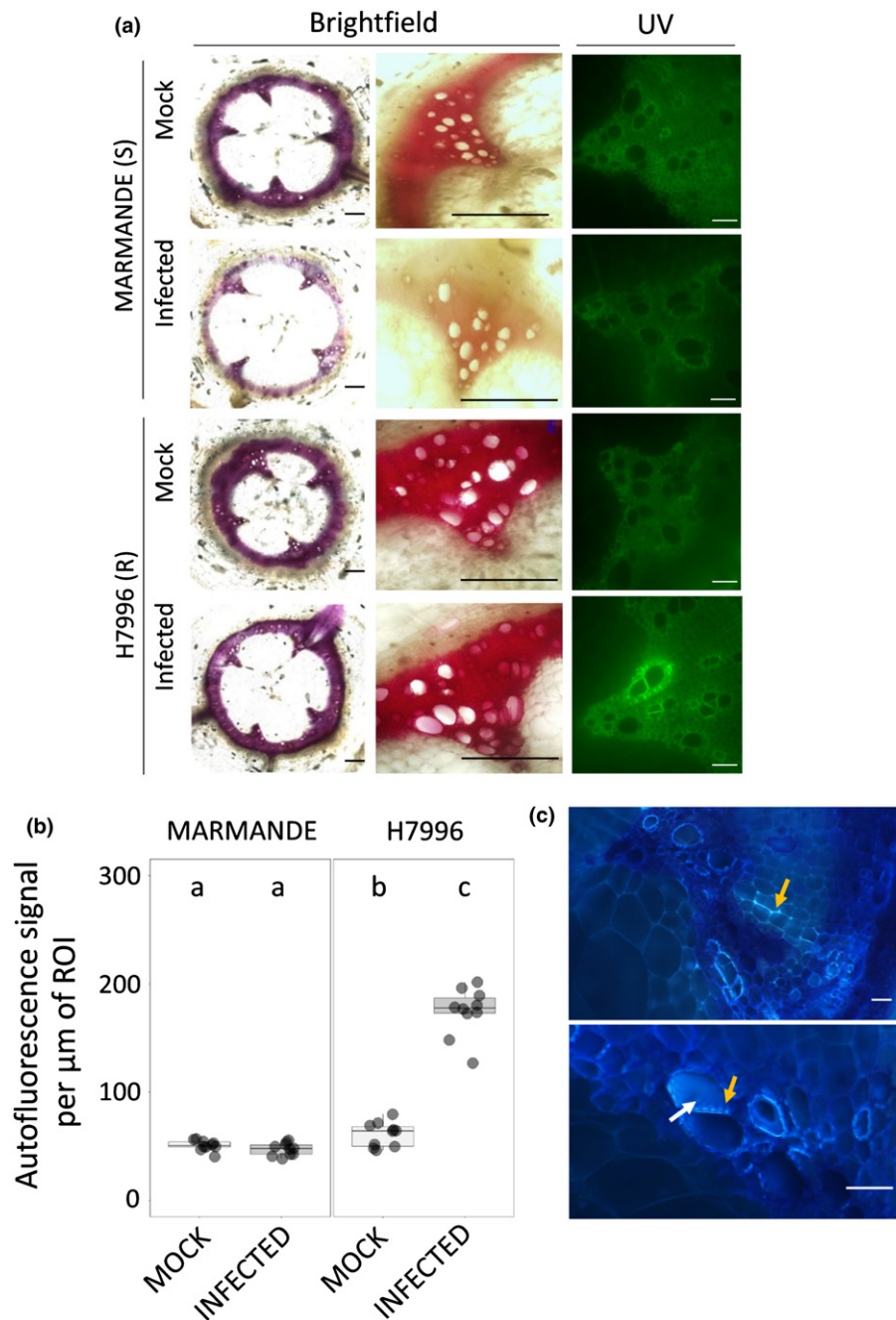
Fig. 3 Resistant H7996 tomato shows vascular autofluorescence not-quenched with phloroglucinol and susceptible Marmande shows a decrease in phloroglucinol-HCl lignin signal. Susceptible (Marmande) and resistant (H7996) 5-wk-old tomato plants were root-inoculated with a *Ralstonia solanacearum* GMI1000 strain at a concentration of *c.* 1×10^7 colony-forming unit (CFU) ml^{-1} or water mock. (a) Cross-sections of the taproot-to-hypocotyl area containing 10^5 CFU g^{-1} of *R. solanacearum* were stained with phloroglucinol-HCl and observed under ultraviolet (UV) to visualize other autofluorescent compounds different from lignin (not quenched with phloroglucinol-HCl) (right) and under brightfield to visualize lignin deposition (left). In infected H7996 strong UV autofluorescence could be observed in the walls of xylem vessels surrounding xylem parenchyma cells and tracheids, indicating reinforcement of walls of vascular tissue with phenolics formed *de novo* upon infection. In infected Marmande the red phlorogucinol stain was reduced especially in the intervessel areas. (b) The UV autofluorescence signal in (a) was measured using the Las X Leica software after the phloroglucinol-HCl treatment. Data are represented with box and whiskers plots: whiskers indicate variability outside the upper and lower quartiles and boxes indicate second quartile, median and third quartile. (c) Detailed observation of infected H7996 xylem after the phloroglucinol-HCl treatment shows the strong UV fluorescence concentrated in specific areas possibly corresponding to intervessel and vessel-parenchyma bordered pit membranes and/or pit chambers (yellow and white arrows, respectively). Fluorescence was also observed in parenchyma cells, specially enriched at intercellular cell corners (green arrow). Panel (b) correspond to a representative experiment out of three each with $n = 6$ plants per variety. Different letters indicate statistically significant differences ($\alpha = 0.05$, Fisher's least significant difference test). Panels (a) and (c) were representative images. Bars: (a, left), 100 μm; (a, right) 500 μm; (c) 50 μm.
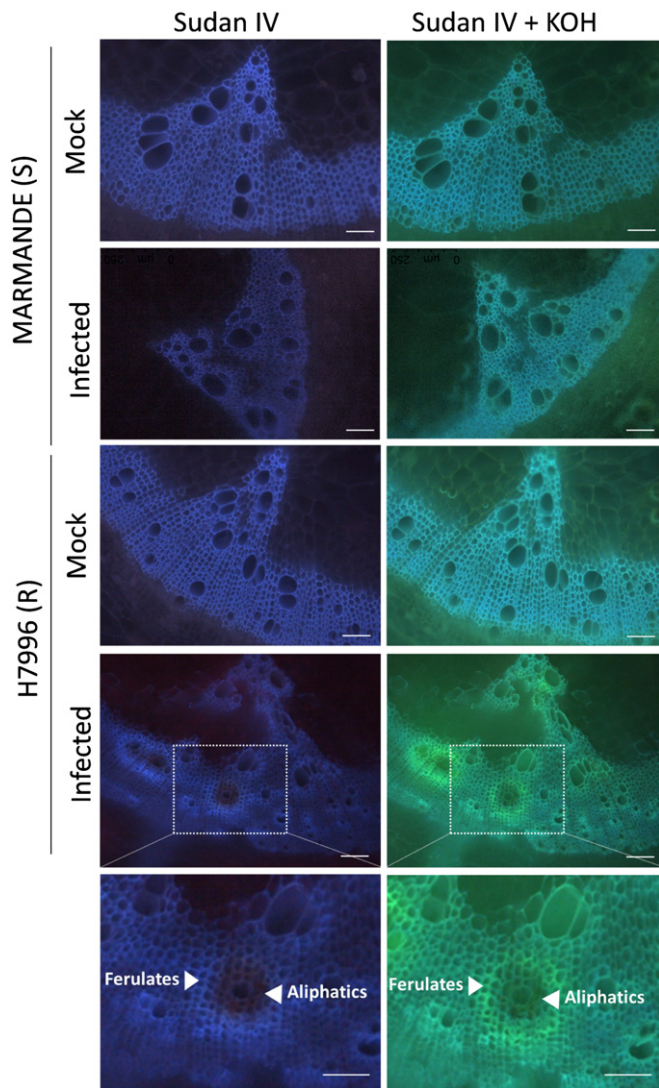
Fig. 4 Resistant H7996 tomato shows cell wall ferulate/feruloylamide and suberin deposition in restricted zones of vascular tissue upon *Ralstonia solanacearum* infection. Susceptible Marmande or resistant H7996 tomato plants were soil-inoculated with a *c.* 1×10^7 colony-forming unit (CFU) ml^{-1} suspension of *R. solanacearum* GMI1000 or mock-inoculated with water and incubated at 28°C. Cross-sections were obtained from taproot-to-hypocotyl transition tissue containing 10^5 CFU g^{-1} of *R. solanacearum*. Sections were stained with Sudan IV to visualize suberin aliphatics and subsequently treated with 1N potassium hydroxide (KOH) (pH above 10) to visualize ferulic acid bound to cell wall. Sudan IV positive staining (reddish-brown coloration) was observed around xylem vessels specifically in infected H7996, indicating accumulation of suberin aliphatics. Accumulation of ferulic acid bound to cell wall (blue-green coloration) appears also specifically in infected H7996 resistant tomato, surrounding Sudan IV-stained areas. White arrowheads indicate the sites of accumulation of ferulates and aliphatic compounds. Representative images from one experiment out of three with $n = 6$ plants each were taken. Bar, 100 μm.

upon *R. solanacearum* infection. Further, these data are in agreement with NMR data of infected H7996, which showed a specific increase in insoluble fatty acid structures typical of suberin as well as the appearance of signals from structural tyramine-derived amides and feruloylamides (Fig. 2a).

Overexpression of *SlTHT1-3* in a susceptible tomato cultivar confers resistance to *R. solanacearum*

Based on our results, we set to determine whether overexpressing genes involved in ferulic acid esterification to suberin aliphatics and feruloylamide biosynthesis, such as *SlFHT* and *SlTHT1-3*, respectively, would increase resistance against *R. solanacearum* in a susceptible tomato background. Initially, we obtained transgenic tomato lines stably overexpressing *SlFHT* on a susceptible Marmande background (Fig. S8). Under normal growth conditions these lines are morphologically undistinguishable from wild-type (Wt), although they display a subtle increase in fresh weight (Fig. S9). We analyzed symptom progression and bacterial colonization. *SlFHT* overexpression lines showed a slight delay in disease progression (Fig. 6a) and moderately milder symptoms. The taproot-to-hypocotyl of *SlFHT* overexpressors displayed a slight reduction in bacterial loads after soil-soak inoculation in comparison to Wt tomato (Fig. 6b).

Regarding *SlTHT1-3*, the corresponding tomato overexpressing line was readily available on a Moneymaker background (Campos *et al.*, 2014). This line has been shown to overaccumulate soluble HCAA such as feruloyltyramine and also the hormone salicylic acid (SA) upon infection with *Pseudomonas syringae* pv. tomato (Campos *et al.*, 2014). It is worth noting that tomato plants overexpressing *SlTHT1-3* display a slight decrease in fresh weight compared to wild-type plants, although with the naked eye they appear undistinguishable (Fig. S10). As expected, the Moneymaker tomato cultivar showed similar susceptibility to *R. solanacearum* as Marmande (Fig. 7a,b). In contrast, overexpression of *SlTHT1-3* resulted in a dramatic increase of resistance against *R. solanacearum*, with disease progressing remarkably slower in this line compared to wild-type (Fig. 7a,b). Importantly, bacterial loads were significantly lower in the taproot-to-hypocotyl and hypocotyl of the *SlTHT1-3* overexpressor after soil inoculation in comparison to Wt tomato (Fig. 7c). Similarly, direct leaf inoculation also showed severe bacterial growth restriction in the *THT1-3* overexpressing line (Fig. S11a). Further, we monitored the colonization patterns of a *R. solanacearum* GFP reporter strain after stem inoculation of the *SlTHT1-3* overexpressing line compared to Wt. In transverse stem cross-sections of 6 dpi plants, bacteria stayed confined near the inoculation point in the *35S::SlTHT1-3* line whereas they spread unrestrictedly in susceptible wild-type stems from the inoculation point and at least 3 cm up and downwards (Fig. 7d,e, S11b).

Concomitant with the observed restriction of *R. solanacearum* colonization, an increase in autofluorescence around the vasculature was observed in the *SlTHT1-3* overexpressor (Fig. 8a). At similar bacterial loads, Wt did not display such enhanced vascular fluorescence. Phloroglucinol-HCl staining did not quench the paravascular autofluorescence in *SlTHT1-3* (Fig. 8a,d), indicating that similar to what was previously observed for H7996, the observed increase in wall-bound phenolic deposits did not only correspond to lignin. To gain a deeper insight into the composition of the *R. solanacearum*-induced vascular deposits in *SlTHT1-3* overexpressing plants we performed combined Sudan IV-alkali staining (Fig. 8b,c,e). Treatment with alkali resulted in a clear
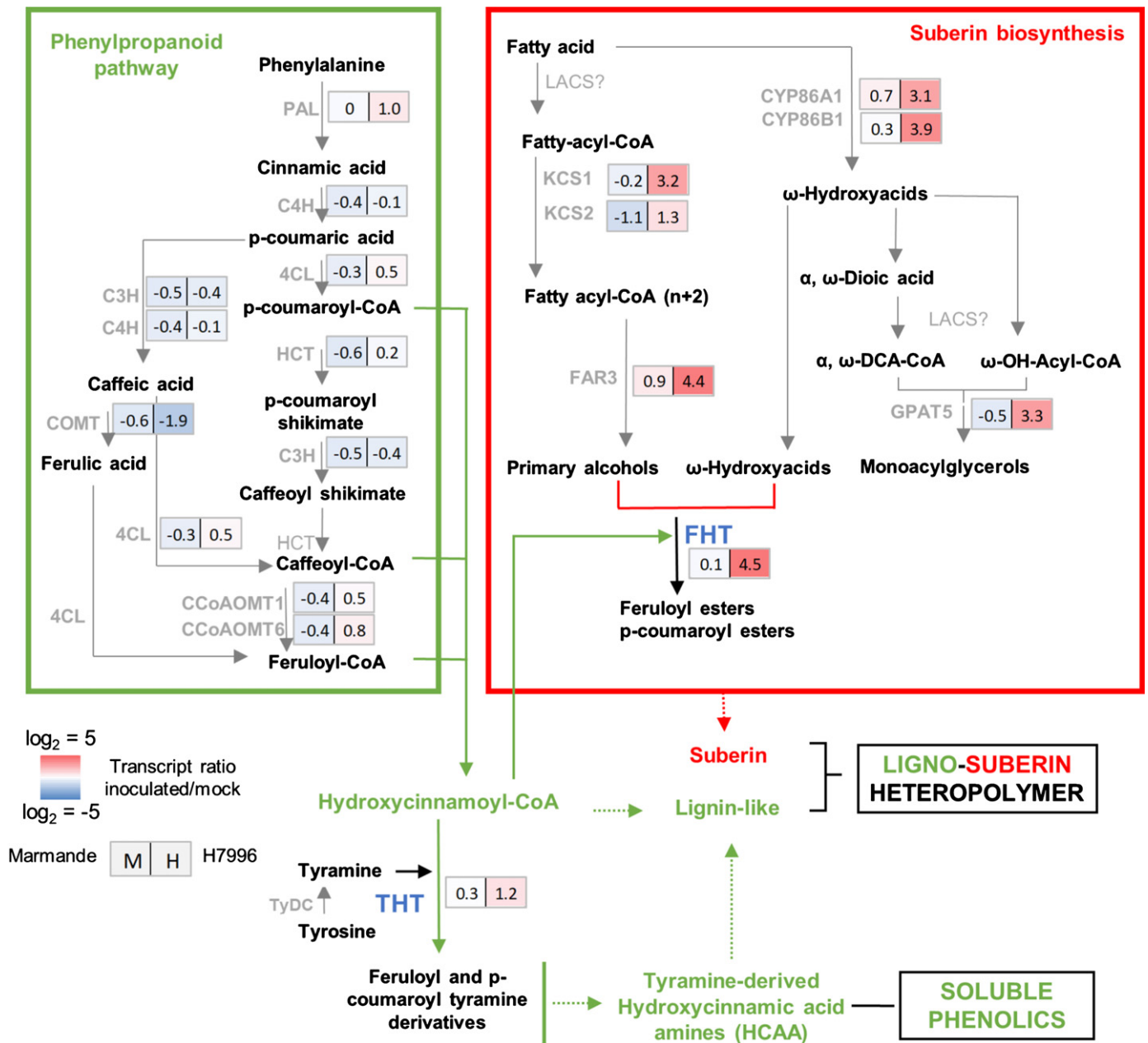
Fig. 5 Genes of the ligno-suberin heteropolymer biosynthesis pathway are specifically induced in the xylem vasculature of resistant H7996 tomato upon *Ralstonia solanacearum* infection. The levels of expression of genes belonging to metabolic pathways relevant for suberin, lignin and feruloyltyramine and related amides biosynthesis were analyzed by quantitative polymerase chain reaction (qPCR) of taproot vascular tissue in infected or mock-treated H7996 or Marmande tomato plants. Plants containing an *R. solanacearum* inoculum of 10^5 colony-forming unit (CFU) g^{-1} were selected and xylem vascular tissue from the taproot-to-hypocotyl transition zone, comprising of metaxylems and surrounding parenchyma cells was collected for RNA extraction and complementary DNA (cDNA) synthesis. In parallel, xylem tissue was collected from mock plants. Heatmaps show $\log_2$ fold change RTA (relative transcript abundance) values of infected vs mock for Marmande (left) and Hawaii (right). The tomato gene encoding for the alpha-subunit of the translation elongation factor 1 (*SleEF1 α*) was used as endogenous reference. Three biological replicates (*n* = 3) were used, and taproots of six plants were used in each replicate. All the original qPCR results can be found in Supporting Information Figs S3–S6. The scheme represents the phenylpropanoid and suberin biosynthesis pathways providing lignin-like and suberin precursors for the ligno-suberin heteropolymer. Abbreviations: PAL, phenylalanine ammonia-lyase; C4H, cinnamate-4-hydroxylase; C3H, coumarate 3-hydroxylase; 4CL, 4-coumarate-CoA ligase; HCT, hydroxycinnamoyl-CoA shikimate/quinate hydroxycinnamoyl transferase; COMT, caffeic acid 3-*O*-methyltransferase; CCoAOMT, caffeoyl CoA 3-*O*-methyltransferase; CYP86A1 and CYP86B1, cytochrome P450 fatty acid ω-hydroxylases; KCS1/2, 3-ketoacyl-CoA synthase; FAR 1/3/4, fatty acyl-CoA reductase; GPAT5, glycerol-3-phosphate acyltransferase 5; THT, tyramine hydroxycinnamoyl transferase; TyDC, tyrosine decarboxylase; FHT, feruloyl transferase. The question mark (?) denotes a hypothetical reaction.
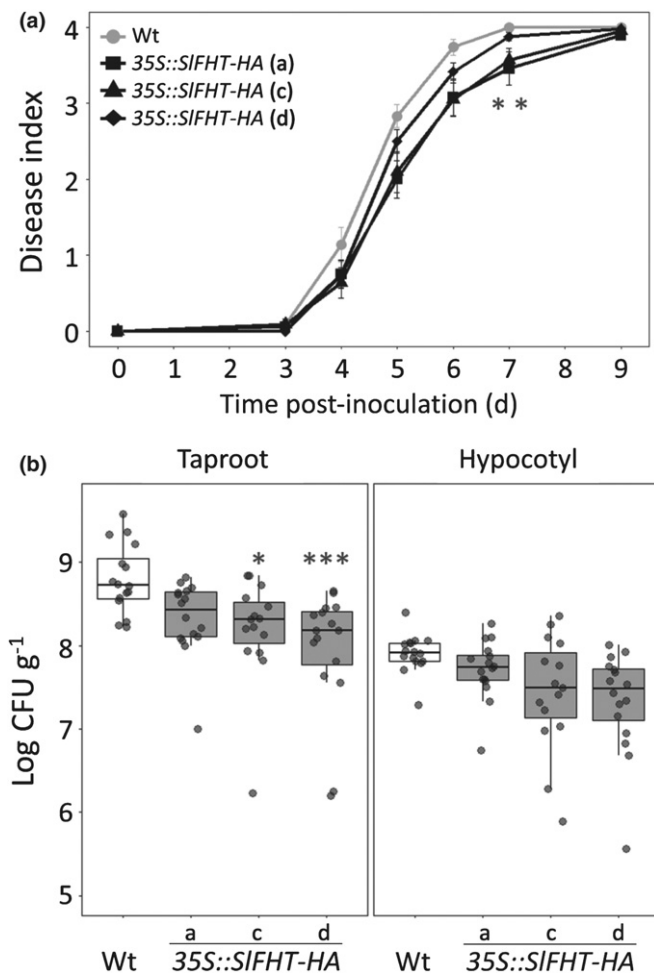
Fig. 6 Overexpression of *SlFHT-HA* in susceptible tomato slightly restricts colonization by *Ralstonia solanacearum*. (a, b) A pathogenicity assay was performed comparing wild-type (Wt) and three independent *35S::SlFHT-HA* Marmande tomato lines (a, c and d) after infection with *R. solanacearum* GMI1000 lux reporter strain. Five-wk-old plants were soil-soak inoculated with c. 1×10^7 colony-forming unit (CFU) ml^{-1} or mock and grown at 28°C. (a) Wilting progress was monitored by rating plants daily on a 0 to 4 disease index scale where 0 = healthy and 4 = 100% wilted. Plotted values correspond to means ± standard error of 24 independent plants ($n = 24$) from a representative experiment out of a total of three. Asterisks indicate statistically significant differences between Wt and each of the *35S::FHT-HA* analyzed using a paired Student's *t*-test (*, $P < 0.05$). (b) The level of *R. solanacearum* colonization in the taproot and hypocotyl was calculated as colony forming units per gram of fresh taproot tissue (CFU g^{-1}) at 12 d post infection (dpi). Data are represented with box and whiskers plots: whiskers indicate variability outside the upper and lower quartiles and boxes indicate second quartile, median and third quartile. Data presented are of a representative experiment out of a total of three experiments. In (a) a Kruskall–Wallis test at each dpi was conducted to examine differences in disease index among different genotypes. Significant differences among genotypes were confirmed by applying a pairwise Wilcox test. Asterisks indicate statistically significant differences between wild-type and *35S::FHT-HA* tomato lines in (a) (*, $P < 0.05$).

blue-to-green shift of UV autofluorescence around xylem vessels occurring specifically in the *SlTHT1-3* overexpressor upon infection, which reveals the presence of ferulates/feruloylamides as part of the observed vascular deposits. In contrast, no positive

Sudan IV staining was detected, indicating that a canonical suberin polyester does not seem to be part of vascular coatings in *SlTHT1-3* overexpressing plants. Since Sudan IV only stains specific moieties of the complex suberin heteropolymer, we cannot rule out that the observed vascular deposits in *SlTHT1-3* are formed by a noncanonical ligno-suberin heteropolymer that does not react with Sudan IV. Further investigation will be needed in order to ascertain the exact nature of the *R. solanacearum-induced* vascular deposits in the *SlTHT1-3* overexpressor. In conclusion, our data clearly show that *StTHT1-3* ectopic expression provides a very effective resistance mechanism against *R. solanacearum* - potentially mediated by accumulation of elevated amounts of HCAAs such as feruloyltyramine, which drastically restricts vascular colonization, preventing bacterial spread and blocking the onset of disease.

Discussion

Ligno-suberin deposits in vascular cell walls and feruloyltyramine accumulation acts as a resistance mechanism restricting *R. solanacearum* colonization in resistant tomato

In our study, resistant tomato (H7996) was observed to react aggressively to *R. solanacearum* infection by reinforcing the walls of vessels and the surrounding parenchyma cells with UV autofluorescent phenolic deposits (Fig. 1). An increase in autofluorescence had been previously reported in another resistant tomato variety, LS-89, although its composition was not precisely defined (Ishihara *et al.*, 2012). Histochemical analysis of vascular coatings in resistant tomato upon *R. solanacearum* infection showed that suberin-associated autofluorescence was prominent in the vasculature, in line with previous reports using transmission electron microscopy (TEM) that showed thickening of the pit membranes accumulating electron-dense material in tomato plants resistant to *R. solanacearum* (Nakaho *et al.*, 2000, 2004). The suberin nature of these coatings was further supported by the positive Sudan IV staining of vessels and surrounding parenchyma cells of H7996 taproot-to-hypocotyl transition zone upon infection (Fig. 4). These results are in agreement with coatings detected in tomato plants resistant to *Verticillium albo-atrum* (Robb *et al.*, 1991), where suberin and lignin were both deposited in intercellular spaces between parenchyma cells adjoining a xylem vessel or infusing and occluding pit membranes coatings (Street *et al.*, 1986; Robb *et al.*, 1991). Besides, inhibition of the phenylpropanoid pathway inhibited the formation of both lignin and suberin coatings (Street *et al.*, 1986), in agreement with the ferulic acid requirement to correctly deposit suberin (Andersen *et al.*, 2021) and reinforcing our observations of the presence of a ferulate/feruloylamide-derived polymer detected in H7996 *R. solanacearum* (Fig. 4). In line with this, NMR data of resistant H7996 tomato vascular tissue revealed the presence of tyramine-derived amides and feruloylamides incorporated into the cell wall and also an enrichment in poly-aliphatic structures characteristic of suberin (Fig. 2) (Graça, 2015; Legay *et al.*, 2016; Figueiredo *et al.*, 2020).
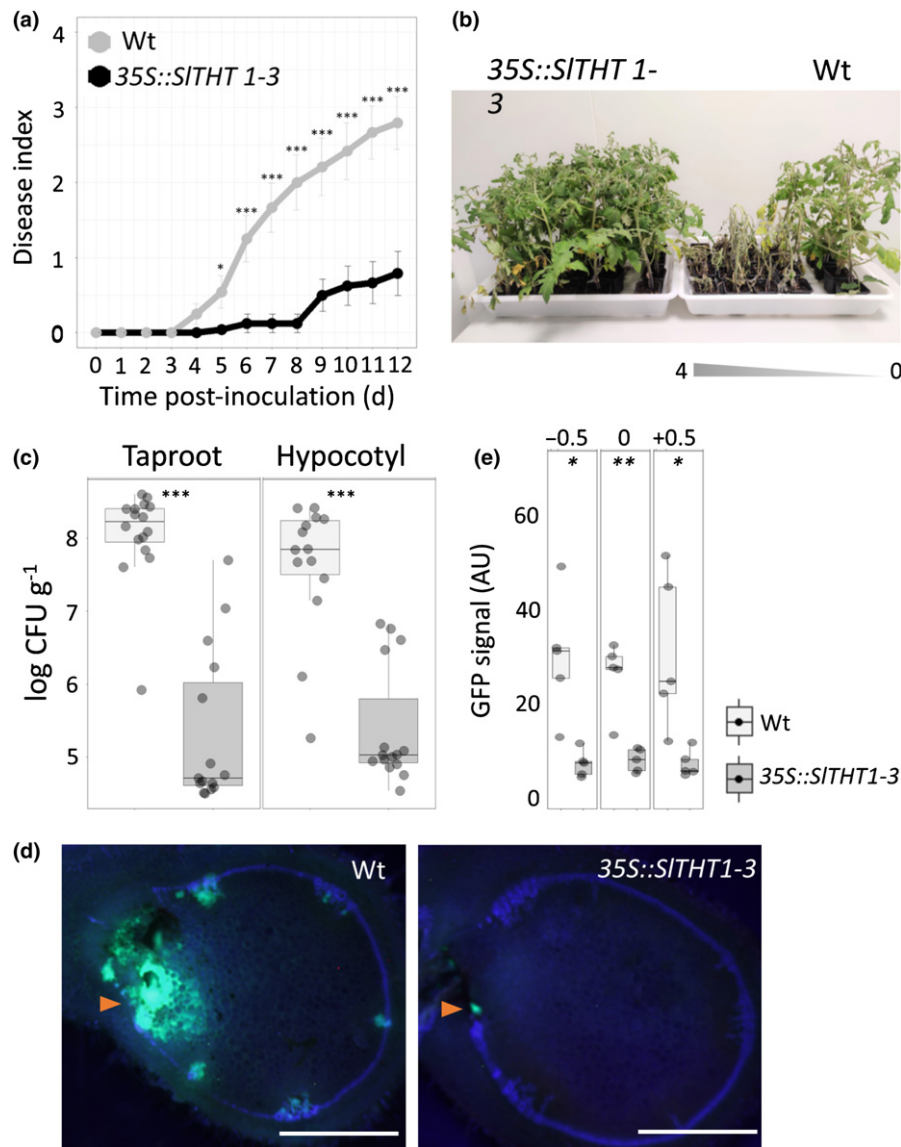
Fig. 7 Overexpression of *SlTHT1-3* in susceptible tomato confers resistance to *Ralstonia solanacearum*. (a, b) A pathogenicity assay was performed comparing wild-type (Wt) and *35S::SlTHT1-3* tomato lines (Moneymaker background) after infection with *R. solanacearum* lux reporter GMI1000 strain. Five-wk-old plants were soil-soak inoculated with *c*. 1×10^7 colony-forming units (CFU) ml^{-1} and grown at 28°C. (a) Wilting progress was monitored by rating plants daily on a 0 to 4 disease index scale where 0 = healthy and 4 = 100% wilted. Plotted values correspond to means ± standard error of 24 independent plants ($n = 24$) from a representative experiment out of a total of three. Asterisks indicate statistically significant differences between Wt and *35S::SlTHT1-3* using a Kruskall–Wallis test at each day post infection (dpi) was conducted to examine differences in disease index among different genotypes. Significant differences among genotypes were confirmed by applying a pairwise Wilcox test (*, $P < 0.05$; ***, $P < 0.0001$). (b) Pictures were taken 12 dpi. Wt plants were arranged according to the degree of symptom severity (from 4 to 0). (c) Transgenic *35S::SlTHT1-3* tomato significantly restricted *R. solanacearum* colonization in both the taproot-to-hypocotyl transition zone and hypocotyl compared to Wt. Five-wk-old tomato plants were root-inoculated with a *R. solanacearum* GMI1000 luciferase reporter strain at a concentration of *c*. 1×10^7 CFU ml^{-1} or water mock. The level of *in planta* colonization by *R. solanacearum* was calculated as colony forming units per gram of fresh taproot tissue (CFU g^{-1}) at 12 dpi. Data are represented with box and whiskers plots: whiskers indicate variability outside the upper and lower quartiles and boxes indicate second quartile, median and third quartile. Box-and-whisker plots show data from a representative experiment out of three ($n = 14$–16) (***, $P < 0.0001$). (d) Transverse stem cross-sections of Wt and transgenic *35S::SlTHT1-3* tomato lines were imaged under a confocal microscope 6 d after infection with a *R. solanacearum* GMI1000 green fluorescent protein (GFP) reporter strain. *Ralstonia solanacearum* at a concentration of 10^5 CFU ml^{-1} was injected directly into the xylem vasculature of the first internode thorough the petiole. Orange arrow points the site of inoculation. Representative images of *R. solanacearum* colonization progress at the point of inoculation are shown. Bar, 2 mm. (e) Mean green fluorescence of the GFP signal emitted from *R. solanacearum* at cross-sections obtained as described in (d) at the point of inoculation (0), below the point of inoculation (−0.5 cm) and above the point of inoculation (+0.5 cm) was measured using IMAGEJ. Data are represented with box and whiskers plots: whiskers indicate variability outside the upper and lower quartiles and boxes indicate second quartile, median and third quartile. Data from a representative experiment out of a total of three, with $n = 5$ plants per condition. In (a) a Kruskall–Wallis test at each dpi was conducted to examine differences in disease index among different genotypes. Significant differences among genotypes were confirmed by applying a pairwise Wilcox test. Asterisks indicate statistically significant differences between wild-type and *35S::SlTHT1-3* tomato lines in (a) (*, $P < 0.05$; **, $P < 0.001$).
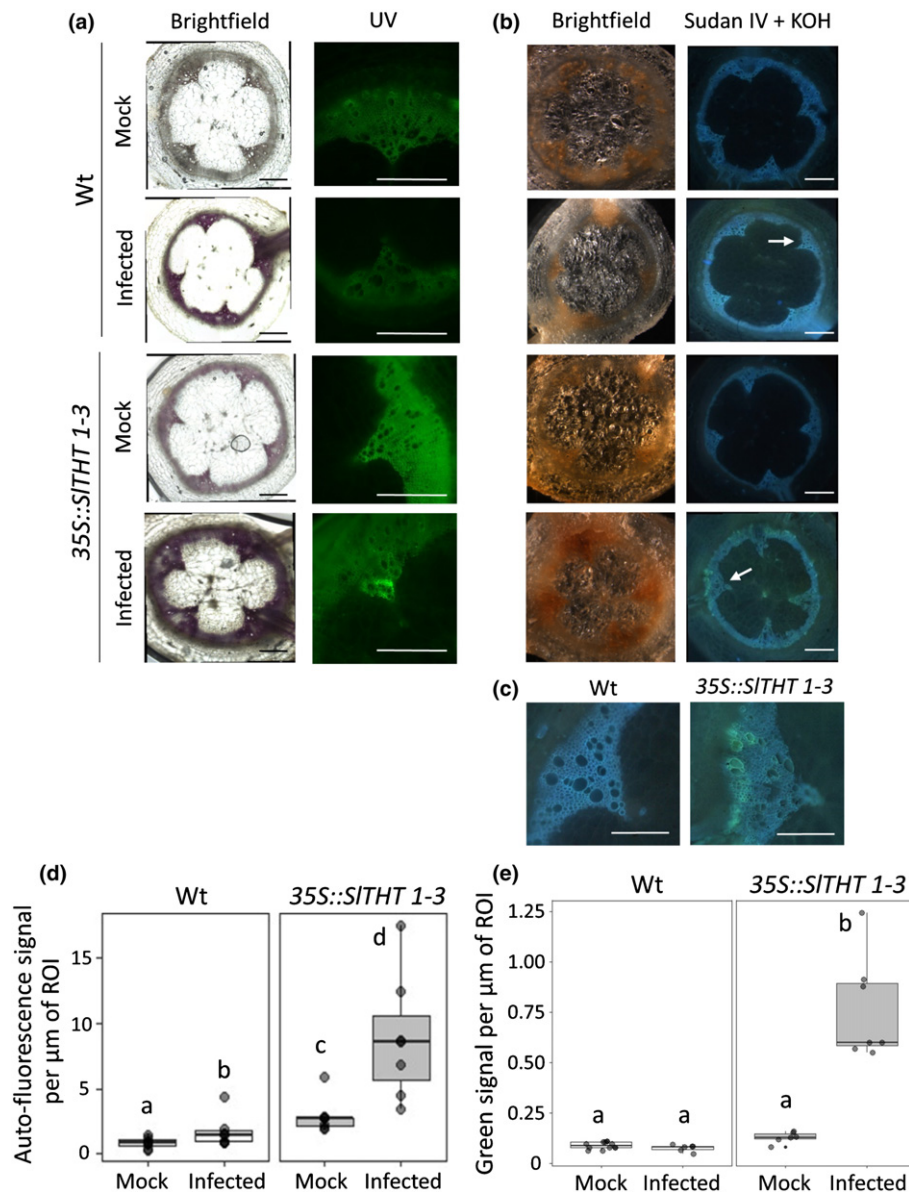
Fig. 8 Overexpression of *SlTHT1-3* in susceptible tomato results in vascular autofluorescence not-quenched with phloroglucinol and cell wall ferulate/feruloylamide deposition in restricted zones of vascular tissue upon *Ralstonia solanacearum* infection. Susceptible wild-type Moneymaker (Wt) or resistant *35S::SlTHT1-3* overxpressing tomato plants were soil-inoculated with a *c.* 1×10^7 colony-forming unit (CFU) ml^{-1} suspension of *R. solanacearum* GMI1000 lux reporter strain. Cross-sections were obtained from taproot-to-hypocotyl of both genotypes tissue containing 10^5 CFU g^{-1} of *R. solanacearum*. (a) Cross-sections were stained with phloroglucinol-HCl and observed under brightfield to visualize lignin deposition (left) and under ultraviolet (UV) to visualize other autofluorescent compounds different from lignin (not quenched with phloroglucionol-HCl) (right). (b) Combined Sudan IV+KOH treatment showed no positive suberin aliphatic signal in *SlTHT1-3*, but a significant increase in ferulate/feruloylamide accumulation upon infection. (c) Close-ups (10×) of the vascular bundles of Wt and *35S::SlTHT1-3* infected plants pointed with a white arrow in (b) are also shown. Images from a representative experiment out of three with $n = 6$ plants per cultivar. (d) Quantification of UV fluorescence after phloroglucinol-HCl staining as shown in (a, right) were performed with Las X software by selecting the vascular areas surrounding main vessels with strong localized fluorescence or green signal. (e) Quantification of UV green fluorescence from ferulate deposits after Sudan IV+KOH staining as shown in (a, right) were performed with Las X software by selecting the vascular areas surrounding main vessels with strong localized fluorescence or green signal. Data in (d, e) are represented with box and whiskers plots: whiskers indicate variability outside the upper and lower quartiles and boxes indicate second quartile, median and third quartile. Different letters indicate statistically significant differences ($\alpha = 0.05$, Fisher's least significant difference test). Bar, 500 μm.

Beyond histochemistry and spectroscopic signature detections, further evidence supporting the nature of these ligno-suberin coatings as responsible of the resistance observed in H7796 to *R. solanacearum* was unequivocally provided transcriptionally using gene markers. Tissues undergoing suberization have to go

through a complex reprogramming involving a network of metabolic pathways, in order to produce the precursors of the polymer and their polymerization into the matrix (Lashbrooke *et al.*, 2016). Transcriptional reprogramming associated to suberin biosynthesis was clearly observed in the taproot-to-

hypocotyl transition zone vascular tissue of resistant H7996 tomato upon infection with *R. solanacearum* (Fig. 5). Interestingly, PAL, which showed modest upregulation in resistant H7996, had been previously defined as a rate-limiting enzyme of phenylpropanoid pathway (Faragher & Brohier, 1984; Howles *et al.*, 1996). Considering this, the observed upregulation could provide more tyramine and feruloyl-CoA, which together with the upregulation of *THT* would be in agreement with the increased presence of feruloyltyramine detected by 2D-HSQC-NMR (Fig. 2a).

The 2D-HSQC-NMR also revealed differences in the composition and structure of lignin between resistant and susceptible tomato cultivars after infection (Fig. 2). The amounts and the level of lignin of a particular tissue affect wall strength, degradability and pathogen resistance (Cho *et al.*, 2012; Mnich *et al.*, 2020). However, its role in resistance/susceptibility responses is not fully understood. Part of the challenge lies in the fact that its composition seems to be less static than what was previously established. A large variety of lignin-like polymers may co-exist in plants depending on the developmental or environmental context. This becomes particularly relevant in plant–pathogen interactions, where a large variety of compounds linked to lignin differentially accumulate upon infection (Cho *et al.*, 2012; Zeiss *et al.*, 2019). The observed lignin structural differences after infection indicate that (1) under basal conditions the two tomato varieties display differences in the composition and structure of lignin and (2) *R. solanacearum* infection affects very differently the lignin fraction in the two varieties: resistant tomato shows only a slight decrease in the S : G ratio that may be linked to an accumulation of the ligno-suberin heteropolymer, while susceptible Marmande undergoes pronounced depolymerization that correlates with a decrease in ferulate/feruloylamide (Fig. 3a). Although *R. solanacearum* has not been shown to be able to specifically depolymerize lignin, the pathogen secretes enzymes that can degrade cell wall polysaccharides and could participate in the observed Marmande stem collapse phenotype (Fig. 1a). In resistant H7996, however, vascular ligno-suberin-containing coatings would allow to create a hydrophobic barrier to prevent enzymes from accessing the cell wall substrates and at the same time create reinforcements, contributing to resistance to the pathogen. The fact that these reinforcements are rich in tyramine/feruloyltyramine, may further reinforce the structural barrier, providing rigidity and hampering cell wall digestibility by the pathogen's hydrolytic enzymes (Macoy *et al.*, 2015a,b; Zeiss *et al.*, 2021). In addition to that, resistant H7996 may have evolved yet undiscovered mechanisms that directly prevent lignin degradation by the pathogen.

Overall, our data indicate that vascular coating with wall-bound ligno-suberized compounds may restrict horizontal spread of the bacterium (Fig. 1). In comparison, susceptible tomato is either not able to induce such vascular coating upon *R. solanacearum* infection or induces a very weak response (Figs 1, 3), potentially predisposing its vascular walls to disruption by the pathogen's cell wall degrading enzymes. Considering that both varieties seem to possess the metabolic components to build such barriers, the difference in response may be a direct effect of the

differential transcriptional activation of the pathway in vascular tissue of H7996 compared to Marmande. The fact that varieties with moderate resistance to *R. solanacearum* show intermediate restriction of colonization (Planas-Marquès *et al.*, 2019), indicate that the formation of these barriers may be a quantitative trait. However, this also opens the possibility that the differential transcriptional activation of the ligno-suberin pathway observed in resistant tomato may have evolved as an effective mechanism to execute defense responses triggered by activation of an immune receptor upon *R. solanacearum* recognition. Very few immune receptors involved in perception of vascular wilt pathogens have been identified so far, and the mechanisms involved in translating this recognition into effective defense responses in the vasculature remain vastly unknown. Considering that the xylem is a dead tissue, it is expected that the surrounding parenchyma cells will have a pivotal role in perception of the pathogen as well as the signaling leading to the synthesis and wall-binding of the metabolites involved in vascular coating structures, such as the one described here. In fact, xylem parenchyma cells have been shown to synthesize vascular coating components in response to the wilt pathogen *V. albo-atrum* (Street *et al.*, 1986). However, how suberin is synthesized and deposited in the xylem is still poorly defined. Exciting research currently ongoing in this area will certainly help understanding the origin and transport of ligno-suberin components to form inducible vascular deposits in response to pathogens. This will also help determine the exact point of perception of the pathogen (at a cell type or tissular level). Identification of pathogen-inducible pathways specifically occurring in resistant varieties such as the one presented here open new avenues of research to shed light on this biologically and agronomically relevant question.

Based on the earlier observations, we propose the following model (Fig. 9). When reaching the xylem vessels of resistant H7996, *R. solanacearum* multiplies and tries to invade the surrounding healthy vessels and parenchyma cells by degradation of the xylem pit membranes and walls. Resistant tomato plants respond to *R. solanacearum* vascular invasion depositing feruloyltyramine and other HCAA-tyramine derived compounds, and suberin. These deposits would block the pit membrane access and serve as coatings of the vessel walls and parenchyma cells present in the immediate vicinity of colonized vessels, compartmentalizing the infection. These ligno-suberized layers together form a 'zone of ligno-suberization' creating a strong physico-chemical barrier to limit *R. solanacearum* spread.

Engineering tomato resistance against *R. solanacearum* by inducing the tyramine-HCAA pathway

Considering the observed accumulation of ligno-suberin and cell wall-linked feruloyltyramine in resistant H7996 tomato in response to *R. solanacearum* infection, we sought to understand the implications of overexpressing genes involved in the synthesis of these compounds in susceptible tomato cultivars upon *R. solanacearum* infection. We focused on *FHT* and *THT* and because their corresponding transcripts are upregulated in the xylem vasculature of resistant tomato upon *R. solanacearum*
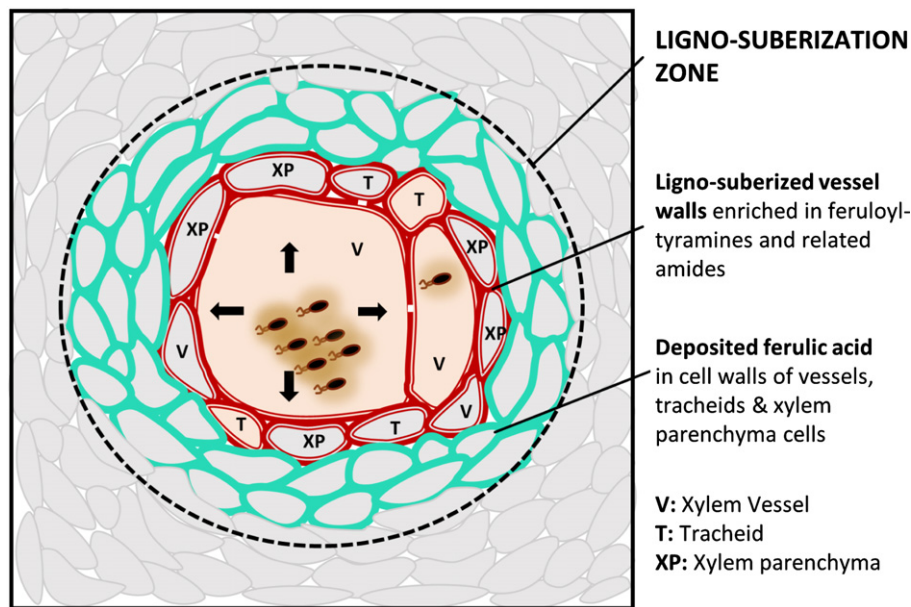
Fig. 9 Schematic representation of the vascular ligno-suberization process potentially taking place in infected vessels of resistant H7996 tomato upon *Ralstonia solanacearum* infection. Colonization of the vasculature by *R. solanacearum* in resistant tomato plants induces a ligno-suberization process in the walls of the infected vessel (V) and of the adjacent tracheids (T) and parenchyma cells (XP) (red). The lignin-like polymer accompanying suberin would be enriched in structural feruloyltyramine and related amides. The signal of structural ferulic acid (ester or as amide) would extend to the walls of peripheral parenchyma cells, vessels and tracheids (green), indicating a stage preceding suberization or a final layered pattern, still to be resolved. Together, the red and green areas, would form a 'zone of ligno-suberization' (black dashed line) potentially creating a physico-chemical barrier to limit *R. solanacearum* spread from the colonized xylem vessel lumen.

infection (Fig. 5) and they are the enzymes related with the synthesis of suberin ferulates and ether linked feruloyltyramine, respectively.

SlFHT overexpression had a small effect on the responses of susceptible tomato against *R. solanacearum*, showing a slight delay in wilting symptoms together with a slight decrease of bacterial loads in the plant (Fig. 6). The fact that increasing the levels of FHT in Marmande does only result in a marginal increase in resistance might be linked to a shortfall of aliphatic precursors in this variety (Fig. 5), which constrain a subsequent increase in suberin synthesis. In contrast, transgenic tomato overexpressing *SlTHT1-3* on a susceptible background was highly resistant to *R. solanacearum* (Fig. 7). Importantly, this transgenic line was previously shown to accumulate elevated amounts of soluble HCAAs such as feruloyltyramine and also SA upon infection with the bacteria *Pseudomonas syringae* pv. *tomato* (*Pto*) and to slightly but significantly restrict bacterial growth (Campos *et al.*, 2014). Since SA does not seem to play a major role in defense responses against *R. solanacearum* (Hirsch *et al.*, 2002; Hernández-Blanco *et al.*, 2007; Hanemian *et al.*, 2016), accumulation of this hormone in *SlTHT1-3* overexpressing line may not be the major underlying cause of the observed increase in resistance in this line. Alternatively, enhanced production of tyramine-derived HCAAs may constitute an important defense strategy against *R. solanacearum*. Feruloyltyramines exhibit antimicrobial activity (Fattorusso *et al.*, 1999; Novo *et al.*, 2017) and that they can be involved in plant priming or an adaptive strategy where plants are in a physiological state with improved defensive capacity (Zeiss *et al.*, 2021). These tyramine-derived

HCAAs overproduced in *SlTHT1-3* overexpressing plants may interfere with *R. solanacearum* colonization by becoming incorporated into the vascular and perivascular cell walls, providing a stronger crosslinking and restricting the movement of the pathogen inside the plant (Fig. 8) but also partly by remaining soluble and acting as direct antimicrobial agents against the pathogen. *Ralstonia solanacearum* possesses a hydroxycinnamic acid degradation pathway and it has been shown that mutants that cannot degrade hydroxycinnamic acids are less virulent on tomato (Lowe-Power *et al.*, 2015; Zhang *et al.*, 2019), which clearly underscores the importance of HCAAs in the arms race taking place in this pathosystem. Considering that the ligno-suberin pathway and HCAAs are well-conserved across the plant kingdom (Philippe *et al.*, 2020; Kashyap *et al.*, 2021; Zeiss *et al.*, 2021), these findings open the possibility to engineer disease resistance in other *R. solanacearum* hosts by manipulating these pathways. Interestingly, ligno-suberin deposits and accumulation of HCAAs have been reported in response to drought (Macoy *et al.*, 2015a,b; Zhang *et al.*, 2020). Therefore, engineering these pathways could have a double impact both on biotic and abiotic stress responses, improving plant performance in the field under adverse conditions.

In conclusion, we have provided evidence of the formation of a 'ligno-suberization zone' enriched in ether-linked feruloyltyramine and possibly related amides as an effective strategy to confine *R. solanacaerum* into infected vessels of resistant tomato plants, preventing horizontal spread of the pathogen into healthy tissues and delaying disease symptoms. Resistance against *R. solanacearum* can be attained in susceptible tomato

background by stably overexpressing *THT* potentially contributing. In the future, it will be interesting to investigate the contribution of HCAAs and suberin to resistance against the pathogen, the mechanisms whereby *R. solanacearum* perception leads to the formation of a ligno-suberin coatings around the vasculature in resistant tomato varieties. Increasing the spatio-temporal resolution of the tomato–*R. solanacearum* interaction will be instrumental to reach a deeper insight into structural resistance mechanisms. Also, since vascular confinement has been reported in different plant species as a means of resistance against various vascular wilt pathogens (De Ascensao & Dubery, 2000; Martín *et al.*, 2008; Xu *et al.*, 2011; Sabella *et al.*, 2018), the level of conservation of vascular ligno-suberin deposition and HCAAs as a constituent of vascular coatings and part of a resistance mechanism remains to be determined.

Author contributions

AK designed and performed experiments, interpreted data and wrote the manuscript. ÁLJ-J performed the experiments required for the second submission of the manuscript. WZ performed experiments. MC performed experiments, interpreted data and reviewed the manuscript. SS conducted preliminary spectroscopy experiments and reviewed the manuscript. JR isolated the lignin/suberin fractions and conducted the 2D-HSQC-NMR analysis, including data interpretation. AG isolated the lignin/suberin fractions and conducted the 2D-HSQC-NMR analysis, including data interpretation. AL conducted preliminary spectroscopy experiments and reviewed the manuscript. OS conducted histopathology staining experiments, interpreted data and reviewed the manuscript. MF interpreted data and reviewed the manuscript. MV designed experiments, interpreted data and reviewed the manuscript. NSC conceptualized the research, designed experiments,

interpreted data and wrote the manuscript. ÁLJ-J and WZ contributed equally to this work.

ORCID

Montserrat Capellades (ID) https://orcid.org/0000-0001-9514-2885
Nuria S. Coll (ID) https://orcid.org/0000-0002-8889-0399
Mercè Figueras (ID) https://orcid.org/0000-0002-6288-1830
Ana Gutiérrez (ID) https://orcid.org/0000-0002-8823-9029
Álvaro Luis Jiménez-Jiménez (ID) https://orcid.org/0000-0002-9406-4595
Anurag Kashyap (ID) https://orcid.org/0000-0003-2622-8209
Anna Laromaine (ID) https://orcid.org/0000-0002-4764-0780
Jorge Rencoret (ID) https://orcid.org/0000-0003-2728-7331
Olga Serra (ID) https://orcid.org/0000-0002-1678-0932
Sumithra Srinivasan (ID) https://orcid.org/0000-0002-0473-9801
Marc Valls (ID) https://orcid.org/0000-0003-2312-0091
Weiqi Zhang (ID) https://orcid.org/0000-0002-2535-1398

Data availability

The data that support the findings of this study are available from the corresponding author upon reasonable request.

References

Álvarez B, Biosca EG, López MM. 2010. On the life of *Ralstonia solanacearum*, a destructive bacterial plant pathogen. In: Méndez-Vilas A, ed. *Technology and education topics in applied microbiology and microbial biotechnology*. Badajoz, Spain: Formatex, 267–279.

Andersen TG, Molina D, Kilian J, Franke RB, Ragni L, Geldner N. 2021. Tissue-autonomous phenylpropanoid production is essential for establishment of root barriers. *Current Biology* 31: 965–977.

Araujo L, Bispo WMS, Cacique IS, Moreira WR, Rodrigues FA. 2014. Resistance in mango against infection by *Ceratocystis fimbriata*. *Phytopathology* 104: 820–833.

Baayen RP, Elgersma DM. 1985. Colonization and histopathology of susceptible and resistant carnation cultivars infected with *Fusarium oxysporum* f. sp. *dianthi*. *Netherlands Journal of Plant Pathology* 91: 119–135.

Benhamou N. 1995. Ultrastructural and cytochemical aspects of the response of eggplant parenchyma cells in direct contact with *Verticillium*-infected xylem vessels. *Physiological and Molecular Plant Pathology* 46: 321–338.

Bernards MA. 2002. Demystifying suberin. *Canadian Journal of Botany* 80: 227–240.

Bernards MA, Lewis NG. 1998. The macromolecular aromatic domain in suberized tissue: a changing paradigm. *Phytochemistry* 47: 915–933.

Bernards M, Lopez M, Zajicek J, Lewis N. 1995. Hydroxycinnamic acid-derived polymers constitute the polyaromatic domain of suberin. *Journal of Biological Chemistry* 270: 7382–7386.

Caldwell D, Kim B, Iyer-Pascuzzi AS. 2017. *Ralstonia solanacearum* differentially colonizes roots of resistant and susceptible tomato plants. *Phytopathology* 107: 528–536.

Campos L, Lisón P, López-Gresa MP, Rodrigo I, Zacarés L, Conejero V, Bellés JM. 2014. Transgenic tomato plants overexpressing tyramine N-hydroxycinnamoyltransferase exhibit elevated hydroxycinnamic acid amide levels and enhanced resistance to *Pseudomonas syringae*. *Molecular Plant–Microbe Interactions* 27: 1159–1169.

Carnachan SM, Harris PJ. 2000. Ferulic acid is bound to the primary cell walls of all gymnosperm families. *Biochemical Systematics and Ecology* 28: 865–879.

Cho K, Kim Y, Wi SJ, Seo JB, Kwon J, Chung JH, Park KY, Nam MH. 2012. Nontargeted metabolite profiling in compatible pathogen-inoculated tobacco

(*Nicotiana tabacum* L. cv. Wisconsin 38) using UPLC-Q-TOF/MS. *Journal of Agriculture and Food Chemistry* **60**: 11015–11028.

Correia VG, Bento A, Pais J, Rodrigues R, Haliński P, Frydrych M, Greenhalgh A, Stepnowski P, Vollrath F, King AWT *et al.* 2020. The molecular structure and multifunctionality of the cryptic plant polymer suberin. *Materials Today Bio* **5**: 100039.

Cruz APZ, Ferreira V, Pianzzola MJ, Siri MI, Coll NS, Valls M. 2014. A novel, sensitive method to evaluate potato germplasm for bacterial wilt resistance using a luminescent *Ralstonia solanacearum* reporter strain. *Molecular Plant–Microbe Interactions* **27**: 277–285.

De Ascensao ARDCF, Dubery IA. 2000. Panama disease: cell wall reinforcement in banana roots in response to elicitors from *Fusarium oxysporum* f. sp. *cubense* race four. *Phytopathology* **90**: 1173–1180.

Digonnet C, Martinez Y, Denancé N, Chasseray M, Dabos P, Ranocha P, Marco Y, Jauneau A, Goffner D. 2012. Deciphering the route of *Ralstonia solanacearum* colonization in *Arabidopsis thaliana* roots during a compatible interaction: focus at the plant cell wall. *Planta* **236**: 1419–1431.

Donaldson L. 2020. Autofluorescence in plants. *Molecules* **25**: 2393.

Donaldson L, Williams N. 2018. Imaging and spectroscopy of natural fluorophores in pine needles. *Plants* **7**: 10.

Falter C, Ellinger D, Von Hulsen B, Heim R, Voigt CA. 2015. Simple preparation of plant epidermal tissue for laser microdissection and downstream quantitative proteome and carbohydrate analysis. *Frontiers in Plant Science* **6**: 194.

Faragher JD, Brohier RL. 1984. Anthocyanin accumulation in apple skin during ripening: regulation by ethylene and phenylalanine ammonia-lyase. *Scientia Horticulturae* **22**: 89–96.

Fattorusso E, Lanzotti V, Taglialatela-Scafati O. 1999. Antifungal N-feruloylamides from roots of two *Allium* species. *Plant Biosystems* **133**: 199–203.

Figueiredo R, Portilla Llerena JP, Kiyota E, Ferreira SS, Cardeli BR, de Souza SCR, dos Santos Brito M, Sodek L, Cesarino I, Mazzafera P. 2020. The sugarcane ShMYB78 transcription factor activates suberin biosynthesis in *Nicotiana benthamiana*. *Plant Molecular Biology* **104**: 411–427.

Gleave AP. 1992. A versatile binary vector system with a T-DNA organisational structure conducive to efficient integration of cloned DNA into the plant genome. *Plant Molecular Biology* **20**: 1203–1207.

Gou J-Y, Yu X-H, Liu C-J. 2009. A hydroxycinnamoyltransferase responsible for synthesizing suberin aromatics in Arabidopsis. *Proceedings of the National Academy of Sciences, USA* **106**: 18855–18860.

Graça J. 2010. Hydroxycinnamates in suberin formation. *Phytochemistry Reviews* **9**: 85–91.

Graça J. 2015. Suberin: the biopolyester at the frontier of plants. *Frontiers in Chemistry* **3**: 62.

Grimault V, Anais G, Prior P. 1994. Distribution of *Pseudomonas solanacearum* in the stem tissues of tomato plants with different levels of resistance to bacterial wilt. *Plant Pathology* **43**: 663–668.

Hanemian M, Barlet X, Sorin C, Yadeta KA, Keller H, Favery B, Simon R, Thomma BPHJ, Hartmann C, Crespi M *et al.* 2016. Arabidopsis CLAVATA1 and CLAVATA2 receptors contribute to *Ralstonia solanacearum* pathogenicity through a miR169-dependent pathway. *New Phytologist* **211**: 502–515.

Harris PJ, Trethewey JAK. 2010. The distribution of ester-linked ferulic acid in the cell walls of angiosperms. *Phytochemistry Reviews* **9**: 19–33.

He M, Ding N. 2020. Plant unsaturated fatty acids: multiple roles in stress response. *Frontiers in Plant Science* **11**: 562785.

Hernández-Blanco C, Feng DX, Hu J, Sánchez-Vallet A, Deslandes L, Llorente F, Berrocal-Lobo M, Keller H, Barlet X, Sánchez-Rodríguez C *et al.* 2007. Impairment of cellulose synthases required for Arabidopsis secondary cell wall formation enhances disease resistance. *Plant Cell* **19**: 890–903.

Hirsch J, Deslandes L, Feng DX, Balagué C, Marco Y. 2002. Delayed symptom development in ein2-1, an Arabidopsis ethylene-insensitive mutant, in response to bacterial wilt caused by *Ralstonia solanacearum*. *Phytopathology* **92**: 1142–1148.

Howles PA, Sewalt VJH, Paiva NL, Elkind Y, Bate NJ, Lamb C, Dixon RA. 1996. Overexpression of L-phenylalanine ammonia-lyase in transgenic tobacco plants reveals control points for flux into phenylpropanoid biosynthesis. *Plant Physiology* **112**: 1617–1624.

Iiyama K, Lam TBT, Stone B. 2020. Covalent cross-links in the cell wall. *Plant Physiology* **104**: 315–320.

Ishihara T, Mitsuhara I, Takahashi H, Nakaho K. 2012. Transcriptome analysis of quantitative resistance-specific response upon *Ralstonia solanacearum* infection in tomato. *PLoS ONE* **7**: e46763.

Jhu M, Farhi M, Wang L, Philbrook RN, Belcher MS, Nakayama H, Zumstein KS, Rowland SD, Ron M, Shih PM *et al.* (2021). Lignin-based resistance to *Cuscuta campestris* parasitism in Heinz resistant tomato cultivars. *bioRxiv*. doi: 10.1101/706861.

Jones JDG, Dangl JL. 2006. The plant immune system. *Nature* **444**: 323–329.

Joo Y, Kim H, Kang M, Lee G, Choung S, Kaur H, Oh S, Choi JW, Ralph J, Baldwin IT *et al.* 2021. Pith-specific lignification in *Nicotiana attenuata* as a defense against a stem-boring herbivore. *New Phytologist* **232**: 332–344.

Kashyap A, Planas-marquès M, Capellades M, Valls M, Coll NS. 2021. Blocking intruders: inducible physico-chemical barriers against plant vascular wilt pathogens. *Journal of Experimental Botany* **72**: 184–198.

Kim SG, Hur OS, Ro NY, Ko HC, Rhee JH, Sung JS, Ryu KY, Lee SY, Baek HJ. 2016. Evaluation of resistance to *Ralstonia solanacearum* in tomato genetic resources at seedling stage. *Plant Pathology Journal* **32**: 58–64.

Lashbrooke J, Cohen H, Levy-Samocha D, Tzfadia O, Panizel I, Zeisler V, Massalha H, Stern A, Trainotti L, Schreiber L *et al.* 2016. MYB107 and MYB9 homologs regulate suberin deposition in angiosperms. *Plant Cell* **28**: 2097–2116.

Legay S, Guerriero G, André C, Guignard C, Cocco E, Charton S, Boutry M, Rowland O, Hausman JF. 2016. MdMyb93 is a regulator of suberin deposition in russeted apple fruit skins. *New Phytologist* **212**: 977–991.

Liu H, Zhang S, Schell MA, Denny TP. 2005. Pyramiding unmarked deletions in *Ralstonia solanacearum* shows that secreted proteins in addition to plant cell-wall-degrading enzymes contribute to virulence. *Molecular Plant–Microbe Interactions* **18**: 1296–1305.

Lowe-Power TM, Ailloud F, Allen C. 2015. Hydroxycinnamic acid degradation, a broadly conserved trait, protects *Ralstonia solanacearum* from chemical plant defenses and contributes to root colonization and virulence. *Molecular Plant–Microbe Interactions* **28**: 286–297.

Lowe-Power TM, Khokhani D, Allen C. 2018. How *Ralstonia solanacearum* exploits and thrives in the flowing plant xylem environment. *Trends in Microbiology* **26**: 929–942.

Lulai EC, Corsini DL. 1998. Differential deposition of suberin phenolic and aliphatic domains and their roles in resistance to infection during potato tuber (*Solanum tuberosum* L.) wound-healing. *Physiological and Molecular Plant Pathology* **53**: 209–222.

Macoy DM, Kim WY, Lee SY, Kim MG. 2015a. Biosynthesis, physiology, and functions of hydroxycinnamic acid amides in plants. *Plant Biotechnology Reports* **9**: 269–278.

Macoy DM, Kim WY, Lee SY, Kim MG. 2015b. Biotic stress related functions of hydroxycinnamic acid amide in plants. *Journal of Plant Biology* **58**: 156–163.

Mahmoud AB, Danton O, Kaiser M, Han S, Moreno A, Algaffar SA, Khalid S, Oh WK, Hamburger M, Mäser P. 2020. Lignans, amides, and saponins from *Haplophyllum tuberculatum* and their antiprotozoal activity. *Molecules* **25**: 2825.

Mangin B, Thoquet P, Olivier J, Grimsley NH. 1999. Temporal and multiple quantitative trait loci analyses of resistance to bacterial wilt in tomato permit the resolution of linked loci. *Genetics* **151**: 1165–1172.

Martín JA, Solla A, Domingues MR, Coimbra MA, Gil L. 2008. Exogenous phenol increase resistance of *Ulmus minor* to Dutch elm disease through formation of suberin-like compounds on xylem tissues. *Environmental and Experimental Botany* **64**: 97–104.

Mazier M, Flamain F, Nicolaï M, Sarnette V, Caranta C. 2011. Knock-down of both eIF4E1 and eIF4E2 genes confers broad-spectrum resistance against potyviruses in tomato. *PLoS ONE* **6**: e29595.

McGarvey JA, Denny TP, Schell MA. 1999. Spatial-temporal and quantitative analysis of growth and EPS I production by *Ralstonia solanacearum* in resistant and susceptible tomato cultivars. *Phytopathology* **89**: 1233–1239.

Mnich E, Bjarnholt N, Eudes A, Harholt J, Holland C, Jørgensen B, Larsen FH, Liu M, Manat R, Meyer AS *et al.* 2020. Phenolic cross-links: building and de-constructing the plant cell wall. *Natural Products Reports* **37**: 919–961.

New
Phytologist

Molina I, Li-Beisson Y, Beisson F, Ohlrogge JB, Pollard M. 2009. Identification of an Arabidopsis feruloyl-coenzyme a transferase required for suberin synthesis. *Plant Physiology* 151: 1317–1328.

Nakaho K, Hibino H, Miyagawa H. 2000. Possible mechanisms limiting movement of *Ralstonia solanacearum* in resistant tomato tissues. *Journal of Phytopathology* 148: 181–190.

Nakaho K, Inoue H, Takayama T, Miyagawa H. 2004. Distribution and multiplication of *Ralstonia solanacearum* in tomato plants with resistance derived from different origins. *Journal of General Plant Pathology* 70: 115–119.

Negrel J, Javelle F, Paynot M. 1993. Wound-induced tyramine hydroxycinnamoyl transferase in Potato (*Solanum tuberosum*) tuber discs. *Journal of Plant Physiology* 142: 518–524.

Negrel J, Pollet B, Lapierre C. 1996. Ether-linked ferulic acid amides in natural and wound periderms of potato tuber. *Phytochemistry* 43: 1195–1199.

Novo M, Silvar C, Merino F, Martínez-Cortés T, Lu F, Ralph J, Pomar F. 2017. Deciphering the role of the phenylpropanoid metabolism in the tolerance of *Capsicum annuum* L. to *Verticillium dahliae* Kleb. *Plant Science* 258: 12–20.

Pérez-Donoso AG, Sun Q, Caroline Roper M, Carl Greve L, Kirkpatrick B, Labavitch JM. 2010. Cell wall-degrading enzymes enlarge the pore size of intervessel pit membranes in healthy and *Xylella fastidiosa*-infected grapevines. *Plant Physiology* 152: 1748–1759.

Philippe G, Sørensen I, Jiao C, Sun X, Fei Z, Domozych DS, Rose JK. 2020. Cutin and suberin: assembly and origins of specialized lipidic cell wall scaffolds. *Current Opinion in Plant Biology* 55: 11–20.

Planas-Marquès M, Bernardo-Faura M, Paulus J, Kaschani F, Kaiser M, Valls M, Van Der Hoorn RAL, Coll NS. 2018. Protease activities triggered by *Ralstonia solanacearum* infection in susceptible and tolerant tomato lines. *Molecular & Cellular Proteomics* 17: 1112–1125.

Planas-Marquès M, Kressin JP, Kashyap A, Panthee DR, Louws FJ, Coll NS, Valls M. 2019. Four bottlenecks restrict colonization and invasion by the pathogen *Ralstonia solanacearum* in resistant tomato. *Journal of Experimental Botany* 71: 2157–2171.

Pomar F, Merino F, Barceló AR. 2002. O-4-linked coniferyl and sinapyl aldehydes in lignifying cell walls are the main targets of the Wiesner (phloroglucinol-HCl) reaction. *Protoplasma* 220: 17–28.

Pomar F, Novo M, Bernal MA, Merino F, Barceló AR, Barceló AR. 2004. Changes in stem lignins (monomer composition and crosslinking) and peroxidase are related with the maintenance of leaf photosynthetic integrity during *Verticillium* wilt in *Capsicum annuum*. *New Phytologist* 163: 111–123.

Potter C, Harwood T, Knight J, Tomlinson I. 2011. Learning from history, predicting the future: the UK Dutch elm disease outbreak in relation to contemporary tree disease threats. *Philosophical Transactions of the Royal Society of London. Series B: Biological Sciences* 366: 1966–1974.

Pouzoulet J, Jacques A, Besson X, Dayde J, Mailhac N. 2013. Histopathological study of response of *Vitis vinifera* cv. Cabernet Sauvignon to bark and wood injury with and without inoculation by *Phaeomoniella chlamydospora*. *Phytopathologia Mediterranea* 52: 313–323.

Pradhan Mitra P, Loqué D. 2014. Histochemical staining of *Arabidopsis thaliana* secondary cell wall elements. *Journal of Visualized Experiments* 87: e51381.

Puigvert M, Guarischi-Sousa R, Zuluaga P, Coll NS, Macho AP, Setubal JC, Valls M. 2017. Transcriptomes of *Ralstonia solanacearum* during root colonization of *Solanum commersonii*. *Frontiers in Plant Science* 8: 370.

Ralph J, Landucci L. (2010). NMR of lignins. In: Heitner JA, Dimmel C, Scmidt DR, eds. *Lignin and lignans: advances in chemistry*. Boca Raton, FL, USA: CRC Press, Taylor & Francis, 137–243.

Razem FA, Bernards MA. 2002. Hydrogen peroxide is required for poly (phenolic) domain formation during wound-induced suberization. *Journal of Agriculture and Food Chemistry* 50: 1009–1015.

Rencoret J, Kim H, Evaristo AB, Gutiérrez A, Ralph J, Del Río JC. 2018. Variability in lignin composition and structure in cell walls of different parts of macaúba (*Acrocomia aculeata*) Palm Fruit. *Journal of Agriculture and Food Chemistry* 66: 138–153.

Rico A, Rencoret J, Del Río JC, Martínez AT, Gutiérrez A. 2014. Pretreatment with laccase and a phenolic mediator degrades lignin and enhances saccharification of *Eucalyptus* feedstock. *Biotechnology for Biofuels* 7: 6.

del Río JC, Rencoret J, Gutiérrez A, Kim H, Ralph J. 2018. Structural characterization of lignin from Maize (*Zea mays* L.) fibers: evidence for diferuloylputrescine incorporated into the lignin polymer in Maize kernels. *Journal of Agriculture and Food Chemistry* 66: 4402–4413.

Rioux D, Nicole M, Simard M, Ouellette GB. 1998. Immunocytochemical evidence that secretion of pectin occurs during gel (gum) and tylosis formation in trees. *Phytopathology* 88: 494–505.

Robb J, Lee SW, Mohan R, Kolattukudy PE. 1991. Chemical characterization of stress-induced vascular coating in tomato. *Plant Physiology* 97: 528–536.

Sabella E, Luvisi A, Aprile A, Negro C, Vergine M, Nicolì F, Miceli A, De Bellis L. 2018. *Xylella fastidiosa* induces differential expression of lignification related-genes and lignin accumulation in tolerant olive trees cv. Leccino. *Journal of Plant Physiology* 220: 60–68.

Salas-González I, Reyt G, Flis P, Custódio V, Gopaulchan D, Bakhoum N, Dew TP, Suresh K, Franke RB, Dangl JL *et al*. 2021. Coordination between microbiota and root endodermis supports plant mineral nutrient homeostasis. *Science* 371: eabd0695.

Schmidt A, Grimm R, Schmidt J, Scheel D, Strackt D. 1999. Cloning and expression of a potato cDNA encoding hydroxycinnamoyl- CoA:tyramine N-(hydroxycinnamoyl)transferase. *Journal of Biological Chemistry* 274: 4273–4280.

Scortichini M. 2020. The multi-millennial olive agroecosystem of salento (Apulia, Italy) threatened by *Xylella fastidiosa* subsp. Pauca: a working possibility of restoration. *Sustain* 12: 6700.

Serra O, Figueras M, Franke R, Prat S, Molinas M. 2010. Unraveling ferulate role in suberin and periderm biology by reverse genetics. *Plant Signaling & Behavior* 5: 953–958.

Serrano M, Coluccia F, Torres M, L'Haridon F, Métraux JP. 2014. The cuticle and plant defense to pathogens. *Frontiers in Plant Science* 5: 274.

Street PFS, Robb J, Ellis BE. 1986. Secretion of vascular coating components by xylem parenchyma cells of tomatoes infected with *Verticillium albo-atrum*. *Protoplasma* 132: 1–11.

Thoquet P, Olivier J, Sperisen C, Rogowsky P, Laterrot H, Grimsley N. 1996. Quantitative trait loci determining resistance to bacterial wilt in tomato cultivar Hawaii 7996. *Molecular Plant–Microbe Interactions* 9: 826–836.

Ursache R, Vieira Teixeira CDJ, Tendon VD, Gully K, Bellis DD, Schmid-Siegert E, Andersen TG, Shekhar V, Calderon S, Pradervand S *et al*. 2021. GDSL-domain proteins have key roles in suberin polymerization and degradation. *Nature Plants* 7: 353–364.

Vasse J, Frey P, Trigalet A. 1995. Microscopic studies of intercellular infection and protoxylem invasion of tomato roots by *Pseudomonas solanacearum*. *Molecular Plant–Microbe Interactions* 8: 241–251.

Vasse J, Genin S, Frey P, Boucher C, Brito B. 2000. The hrpB and hrpG regulatory genes of *Ralstonia solanacearum* are required for different stages of the tomato root infection process. *Molecular Plant–Microbe Interactions* 13: 259–267.

Wang JF, Ho FI, Truong HTH, Huang SM, Balatero CH, Dittapongpitch V, Hidayati N. 2013. Identification of major QTLs associated with stable resistance of tomato cultivar "Hawaii 7996" to *Ralstonia solanacearum*. *Euphytica* 190: 241–252.

Xu L, Zhu L, Tu L, Liu L, Yuan D, Jin L, Long L, Zhang X. 2011. Lignin metabolism has a central role in the resistance of cotton to the wilt fungus *Verticillium dahliae* as revealed by RNA-seq-dependent transcriptional analysis and histochemistry. *Journal of Experimental Botany* 62: 5607–5621.

Yadeta KA, Thomma BPHJ. 2013. The xylem as battleground for plant hosts and vascular wilt pathogens. *Frontiers in Plant Science* 4: 97.

Zeiss DR, Mhlongo MI, Tugizimana F, Steenkamp PA, Dubery IA. 2019. Metabolomic profiling of the host response of tomato (*Solanum lycopersicum*) following infection by *Ralstonia solanacearum*. *International Journal of Molecular Sciences* 20: 3945.

Zeiss DR, Piater LA, Dubery IA. 2021. Hydroxycinnamate amides: intriguing conjugates of plant protective metabolites. *Trends in Plant Science* 26: 184–195.

Zhang L, Merlin I, Pascal S, Bert PF, Domergue F, Gambetta GA. 2020. Drought activates MYB41 orthologs and induces suberization of grapevine fine roots. *Plant Direct* 4: 278.

Zhang Y, Zhang W, Han L, Li J, Shi X, Hikichi Y, Ohnishi K. 2019. Involvement of a PadR regulator PrhP on virulence of *Ralstonia solanacearum* by controlling detoxification of phenolic acids and type III secretion system. *Molecular Plant Pathology* 20: 1477–1490.

Zuluaga AP, Solé M, Lu H, Góngora-Castillo E, Vaillancourt B, Coll N, Buell CR, Valls M. 2015. Transcriptome responses to *Ralstonia solanacearum* infection in the roots of the wild potato *Solanum commersonii. BMC Genomics* 16: 246.

Supporting Information

Additional Supporting Information may be found online in the Supporting Information section at the end of the article.

Fig. S1 Tissue used for analysis and bacterial dynamics.

Fig. S2 H7996 plants show mild symptoms upon challenge inoculation of *Ralstonia solanacearum*.

Fig. S3 Vascular coating response to *Ralstonia solanacearum* infection with wall bound phenolics.

Fig. S4 Expression of suberin biosynthetic genes in xylem vasculature of taproots upon infection of *Ralstonia solanacearum*.

Fig. S5 Phylogeny of feruloyl transferase (FHT) orthologs in different plant species and expression of the putative tomato FHT ortholog in response to *Ralstonia solanacearum* infection.

Fig. S6 Phylogeny of tyramine hydroxycinnamoyl transferase (THT) orthologs in different plant species and expression of the tomato THT gene family members in response to *Ralstonia solanacearum* infection.

Fig. S7 Expression of phenylpropanoid pathway genes in xylem vasculature of taproots upon invasion of *Ralstonia solanacearum*.

Fig. S8 Immunoblot of *35S::SlFHT-HA* in independent Marmande tomato lines expressing *35S::SlFHT-HA* (Marmande).

Fig. S9 Fresh weight of *35S::SlFHT-HA* plants.

Fig. S10 Fresh weight of *35S::SlTHT1-3* plants.

Fig. S11 Overexpression of *SlTHT1-3* in tomato results in restricted colonization by *Ralstonia solanacearum*.

Table S1 List of primers used in this study.

Table S2 Assignments of the correlation signals in the two-dimensional heteronuclear single quantum coherence (2D HSQC) spectra.

Please note: Wiley Blackwell are not responsible for the content or functionality of any Supporting Information supplied by the authors. Any queries (other than missing material) should be directed to the *New Phytologist* Central Office.